University of Alberta

Library Release Form

Name of Author: Antony Roth

Title of Thesis: The Effect of Breathing Pattern on Nebulizer Drug Delivery

Degree: Master of Science

Year this Degree Granted: 2001

"All that I have seen readies me to trust the Creator for all I have not seen."

–Ralph Waldo Emerson

"It is only with the heart that one can see rightly;
what is essential is invisible to the eye."

–Antoine de Saint-Exupéry

University of Alberta

The Effect of Breathing Pattern on Nebulizer Drug Delivery

by

Antony Roth 

A thesis submitted to the Faculty of Graduate Studies and Research in partial fulfillment of the requirements for the degree of **Master of Science**.

Department of Mechanical Engineering

Edmonton, Alberta
Fall 2001

University of Alberta

Faculty of Graduate Studies and Research

The undersigned certify that they have read, and recommend to the Faculty of Graduate Studies and Research for acceptance, a thesis entitled **The Effect of Breathing Pattern on Nebulizer Drug Delivery** submitted by Antony Roth in partial fulfillment of the requirements for the degree of **Master of Science**.

To my family for their complete support and love. I am who I am because of them.
To my Lord and Saviour from whom my gifts come.

Abstract

A rigorous study of the significance of using simplified breathing patterns in vented jet nebulizer research is presented. This research is divided into three parts beginning with the collection of normal and nebulizer human breathing patterns and comparison with simple sine and square waveforms. The isolated breathing patterns are subsequently tested in two ways, through *in vitro* bench testing and an Eulerian computer program (TechAero) simulating the aerosol flow in a modelled human lung.

Comparing nebulizer to normal human breathing revealed significant changes, including an increase in the period and tidal volume, and a shift towards a more symmetrical duty cycle. Bench tests uncovered no significant differences in nebulizer output efficiency in most cases and TechAero simulations produced insignificant dosage differences arising from breathing pattern variation. However, combining the simulation and bench test results reveal that using square waves significantly overpredicts the lung dosage as a percentage of the initial nebulizer charge.

Acknowledgements

Thanks to Dr. Warren Finlay for his direction and patience during the completion of this manuscript. Many thanks also go out to Dr. Carlos Lange for his insight, guidance, and leadership throughout my many questions and interruptions of his work. Recognition and thanks also go out for the laboratory aid of Helena Orszanska and the helpful discussions with my colleagues Wes Dehaan, Tejas Desai, Biljana Grgic, and Austin Voss. Finally, gracious thanks for the financial support of the Natural Sciences and Engineering Research Council of Canada.

Contents

List of Figures

List of Tables

Chapter 1

Introduction

1.1 Preamble

Aerosols, defined as a liquid or solid colloidal mixture in a gas, are always present in the air we breathe and are continuously being inhaled and exhaled by humans. Airborne particulate matter depositing in the lungs can introduce pathogens into the human body as well as impair normal physiological transport processes. As a result, the respiratory tract is designed to minimize the amount of particles depositing and to clear those particles that do deposit. If a particle is small ($\sim 0.3\mu$m) it will be inhaled and exhaled with little deposition, while if a particle is large ($\sim 10\mu$m and larger) it will impact in the upper airways and be removed by the muco-ciliary transport system. Particles in the size range between 1 to 6μm, however, have a higher probability of depositing in the lungs and being absorbed by the body.

Having particles deposit in the lungs can be very desirable in the case of medical applications. At present, aerosolized drugs are used in the treatment of many respiratory diseases such as asthma, cystic fibrosis, and chronic obstructive pulmonary disorder (COPD). The advantages of aerosol drug delivery also make this an attractive option to deliver drugs for regular systematic treatment such as administering morphine as an analgesic or for routine insulin delivery for diabetics.

Delivering drugs to the lungs using therapeutic aerosols has several advantages over other methods. Aerosol drug delivery strikes an appropriate balance between the convenience and safety of oral methods, which are generally slow and non-localized, to the rapid and controlled action of intravenous methods, which are inconvenient and require trained personnel to administer. Aerosol drug delivery offers advantages of both of these other methods. It is

safe and easy, while the localized application results in decreased amounts of drug needed and a decreased chance of adverse reactions. However it is not without drawbacks; the actual delivered dose is often variable and unpredictable while lung disease and severe obstructions may restrict the ability of the drug to penetrate deep enough into the lung to be effective [2].

Research in the field of aerosol drug delivery has developed a greater understanding of the underlying physical principles of aerosol generation in various devices as well as the laws governing the behaviour and deposition tendencies of particles in the respiratory tract. However, the process is exceedingly complex and much more is left to be learned and understood.

1.2 Reasons for Research

With the goal of improving device design to enhance the efficacy of therapeutic aerosols or simply to understand the relevant physical principles, aerosol drug delivery is tested in several ways. Clinical trials can be done *in vivo* with the dependent variable being the therapeutic effect on the patient. Alternatively, *in vivo* tests may include radiolabeled particles and gamma camera techniques to allow a measure of regional particle deposition. These methods have their uses but can be costly and time consuming. It is often more desirable to perform simple bench tests that allow for consistent repetitive testing, demanding less time and money, and enabling isolation of specific factors for scrutiny. The most common *in vitro* laboratory tests involve a mechanical breath simulator inhaling aerosol from the device with the inhaled aerosol collected on a filter for later assay.

Aerosol drug delivery is also commonly tested using computer simulations. In general, the resultant differential equations obtained by representing the problem by the physical laws governing the flow are solved mathematically for modelled lung geometries. However, both lab testing and computer simulation are similar in their attempt to gain knowledge about real physical phenomenon by their use of a simplified model. It would be a wasteful process, however, to develop a test method, perform the experiment and analyze the results only to discover that they are essentially worthless because they do not sufficiently represent reality.

It is critical to realize that experiments performed *in vitro* must simulate reality as near

as possible [3,4]. Clearly, the more assumptions and simplifications that are made, the less certain we can be that the actual *in vivo* situation is being accurately simulated. Additionally, there is also a need to develop consistent and comparable bench testing methods. Different researchers will have different opinions as to what are acceptable assumptions and simplifications and this can then lead to difficulties in comparing results from one research group to another. More important, however, are the differences that occur as the result of separate laboratories performing similar tests under different conditions. While experiments performed in different labs may independently be technically sound with all variables held fixed except the one under test, differences in the test methods themselves can produce varying results.

The need for testing standardization is exemplified by methods used for assaying drug amounts remaining in nebulizers (see section 2.3 on page 9) after nebulization is complete. With a known amount and concentration of drug solution placed in the nebulizer bowl, the drug remaining after complete nebulization has been calculated gravimetrically by some researchers by simply weighing the nebulizer before and after the test. It was later discovered, however, that, during nebulization, evaporation of the solvent continuously occurs resulting in a more concentrated drug solution at the end of the process. Consequently, the gravimetric method can grossly overestimate drug output [5–7]. As a result, comparisons between researchers using gravimetric assay techniques to those using more direct assaying methods were rendered meaningless.

Another example of the need for testing standardization is seen in the variability of breathing patterns used in nebulizer testing. In the testing of medical jet nebulizers, a breathing pattern is usually implemented by a ventilator or mechanical breath simulator to "inhale" the aerosol onto a filter or through a test airway geometry. In some cases, the flow pattern used has a sine wave shape [4,8] and in other cases a square wave pattern is used [9]. On occasion, an attempt is made at using a "real" breathing pattern obtained from measuring a human subject's breathing [4]. Is it also common for only the typical breath parameters to be specified with no clear mention of the functional shape of the breath pattern used [10,11]. The most commonly specified parameters include the tidal volume, defined as the volume of air inhaled with each breath, the frequency, defined as the number

of breaths per minute, and duty cycle, defined as the inhalation time divided by the period. In two separate studies, simplified breathing patterns were used that most closely mimicked real human tidal breathing [4, 9]. Unfortunately, in one case a sine wave was chosen while in the other, a square wave. In light of all this, it is surprising that researchers in the field acknowledge that the flow pattern implemented can have an effect on the output aerosol from the device and correspondingly the resultant deposition patterns [1, 3, 4, 8, 11–14].

Breathing pattern differences involving tidal volume, frequency, and duty cycle may in themselves appear to cause differences in drug delivery if not isolated correctly [12]. However, changes to those parameters are secondary if there is a resultant change in minute ventilation, defined as the total volume of air inhaled in a minute. Increases in drug deposition would then largely be the consequence of an increase in minute ventilation. In other words, more drug is collected because more air and drug is being inhaled due to the larger minute ventilation and not specifically because of differences in tidal volume, period or duty cycle.

In this thesis we wish to examine the effect that the functional shape of the breathing waveform has on vented nebulizer drug delivery. We hypothesize that the flow pattern waveshape can affect nebulizer drug delivery in two ways. Breathing pattern variations can affect 1) the output of a vented jet nebulizer, characterized in terms of the total amount and the particle size distribution of drug exiting the device in addition to 2) the deposition probabilities of the drug particles once inhaled. To our knowledge there has been no published examination of the magnitude or significance of these specific effects.

Chapter 2

Background

2.1 Introduction

This chapter provides some background information pertaining to nebulizers and aerosol drug delivery. It should aid in understanding some of the major concepts relevant to this field as well as providing a clearer perspective of the motivation for this research.

2.2 Factors Influencing the Delivery of Aerosolized Drugs

The factors that influence where a particle will end up depositing in the respiratory tract can be looked at from two perspectives. Generally speaking, deposition probability is greatly influenced by the delivery device used and the manner in which it is employed. From the viewpoint of the physics and fluid dynamics governing the flow, however, the base factors affecting aerosol drug delivery are 1) the size of the particle, 2) the airflow carrying the particle, and 3) the actual structure of the airway itself. This report will specifically examine the effect of breathing pattern on the factors listed above.

2.2.1 Airway Geometry

The effect due to airway structure creates a great challenge in the study of inhalation aerosols as it is virtually impossible to precisely simulate a human lung in the lab. To begin with, the human respiratory tract at the alveolar level is so minutely featured that it cannot be represented accurately to any real extent. Large interpersonal variability combined with the time varying nature of the human lung necessitate a major simplification in the study of aerosol drug delivery. Any sort of test or simulation in the lab must consider an idealized

model lung geometry. In addition, the effect of lung disease on the geometry of the airways is usually not even considered and would tend to push the model even farther from reality.

Traditionally, the lung has been represented as a constant system of bifurcating cylindrical tubes of specified length and diameter. Each successive bifurcation creates a new airway generation with twice as many tubes of smaller length and diameter. This way of considering lung geometry was pioneered by E.R. Weibel in 1963 and his first attempt to model the human airway has been termed the Weibel A lung. Since then, improvements to the original Weibel lung have been suggested to remove simplifications and to correct inherent flaws in the original model. These changes included altering the lengths and diameters of different generations of the lung, introducing more realistic asymmetry into the bifurcations, as well as debating where each of the major lung sections (i.e. extrathoracic, tracheobronchial, and alveolar) should begin and end. While simplifications will always need to be made it is important that laboratory testing continue to strive to decrease its distance from reality.

2.2.2 Particle Size and Airflow in the Respiratory Tract

For a given lung geometry, particle size and the airflow pattern concurrently determine where a particle ends up in the respiratory tract. The main mechanisms causing a particle to deposit in the lung are gravitational sedimentation, inertial impaction, and molecular diffusion. All of these mechanisms contain a dependency on both the size of the particle and the carrier airflow.

2.2.2.1 Inertial Impaction

As air flows through the respiratory tract the flow must continually change direction to follow the branching airways. The drag on droplets entrained in the flow will try to keep the particles following fluid streamlines as they change direction. However, if a particle is too large for a given flow velocity, inertial forces overcome the drag forces and the particle will no longer be able to follow the streamlines. As a result, the particle will impact on the walls of the airway. This tendency to remain entrained in the flow can be characterized by the Stokes number shown in Equation 2.1.

$$Stk = \frac{\rho d^2 U C_c}{18 \mu D} \tag{2.1}$$

where Stk — particle Stokes number;
ρ — particle density [kg/m^3];
d — particle diameter [m];
U — flow velocity [m/s];
C_c — Cunningham slip correction factor;
μ — bulk fluid viscosity [kg/m·s];
D — characteristic dimension of lung generation [m];

Due to the dependence on d and U, variations in both particle size and flow velocity can alter the probable deposition location of a particle. In general, particles with a Stokes number much less than 1 are able to follow the flow, while particles with a Stokes number of order 1 are not able to follow the fluid streamlines and will impact. Analysis of the Stokes number for typical values of the above variables shows that inertial impaction is most significant in the upper airways [2].

2.2.2.2 Sedimentation

Under the acceleration of gravity, a particle will accelerate downwards until it reaches its terminal or settling velocity. If a particle remains resident in a given generation for sufficient time, it will travel far enough to reach the wall of the tube and deposit there. The settling velocity can be derived from a balance between the opposing drag and gravity forces acting on a particle and is given for the low Reynolds number flows commonly found in the respiratory tract as Equation 2.2.

$$v_s = \frac{\rho g C_c d^2}{18 \mu} \tag{2.2}$$

where v_s — particle settling velocity;
ρ — particle density [kg/m^3];
g — gravitational acceleration [m/s^2];
C_c — Cunningham slip correction factor;
d — particle diameter [m];
μ — bulk fluid viscosity [kg/m·s];

The settling velocity is then incorporated into a dimensionless sedimentation parameter, ϵ shown in Equation 2.3. It is this sedimentation parameter that characterizes the tendency of particles to deposit via sedimentation within a particular generation.

$$\epsilon = \frac{3v_s L \cos(38.25°)}{4D\overline{U}} \tag{2.3}$$

where ϵ — sedimentation parameter;
v_s — particle settling velocity [m/s];
L — length of generation [m];
D — diameter of generation [m];
$\overline{U}$ — average flow velocity in generation [m/s];

It is clear that both Equations 2.2 and 2.3 contain a dependency on the flow rate and the diameter of the particle. As the particle size increases, the settling velocity also increases. The flow velocity carrying the particle affects deposition by influencing the residence time in each lung generation. A detailed consideration of typical values for the above variables in different lung sections indicate that sedimentation would be most significant in the deepest sections of the lung [2].

2.2.2.3 Diffusion

The natural and random Brownian motion of particles may be a factor in the deposition of very small particles (typically $<1\mu$m). The tendency for a particle to diffuse to the lung walls and deposit can be characterized by Equation 2.4, the diffusion parameter.

$$h = \frac{kTLC_c}{3\pi\mu d D^2 \overline{U}} \tag{2.4}$$

where h — diffusion parameter;
k — Boltzmann's constant [J/K];
T — gas temperature [K];
L — length of lung generation [m];
C_c — Cunningham slip correction factor;
μ — bulk fluid viscosity [kg/m·s];
d — particle diameter [m];
D — diameter of lung generation [m];
$\overline{U}$ — average flow velocity [m/s];

Again, the deposition probability contains a dependence on both the airflow and the particle size. Examining typical values for the diffusion parameter indicate that deposition by diffusion may be a factor for small particles in the most distal reaches of the lung [2].

2.2.3 Delivery Device

As stated above, the specific device and its usage have a great effect on aerosol drug delivery. In general, there are three types of aerosol delivery devices. 1) Metered dose inhalers (MDI) operate by way of a pressurized canister discharging a single burst of spray for each use. The device releases a metered amount of drug contained in the propellant used to drive the jet and needs to be coordinated with the user's inhalation. 2) Dry powder inhalers (DPI) contain drug in powder form which is drawn into the lungs by the force of the user's inspiration. 3) Jet nebulizers use the principle of two fluid atomization to generate aerosol droplets from an aqueous solution containing the drug to be delivered. Whereas the first two devices deliver a single dose with each actuation, a nebulizer is generally intended for administration of larger drug doses over a longer period of time during continuous tidal breathing.

Jet nebulizers can also be subdivided into two more classes shown in Figure 2.1: vented and unvented. Both types of nebulizer function on the same principles, but an unvented (also termed constant output) nebulizer entrains its output aerosol into the inhaling airflow by way of a T junction. A vented, or breath enhanced, nebulizer actually draws all the inhaled air in through the body of the device. Therefore, unvented nebulizer output into the T junction is independent of the inhalation airflow and only vented jet nebulizers will be considered in this report. The other aspect of this problem, namely the effect of airflow on the deposition probabilities, would be common to both unvented and vented jet nebulizers. Thus, even though this report only examines the effect of flow pattern on a vented jet nebulizer, the results of the effects of flow pattern on the regional dosages can be extended to include unvented jet nebulizers.

2.3 Vented Jet Nebulizer Structure and Function

The airflow through a vented jet nebulizer can affect the aerosol output in two ways. It can affect the particle size distribution as well as the total amount of aerosol that is output and available for inhalation. Of course, many factors, including compressor flow rate, fill volume, solution viscosity and surface tension, and temperature and humidity of ambient air will affect nebulizer output in these same ways [7,8,10,15,16]. But by ensuring all these

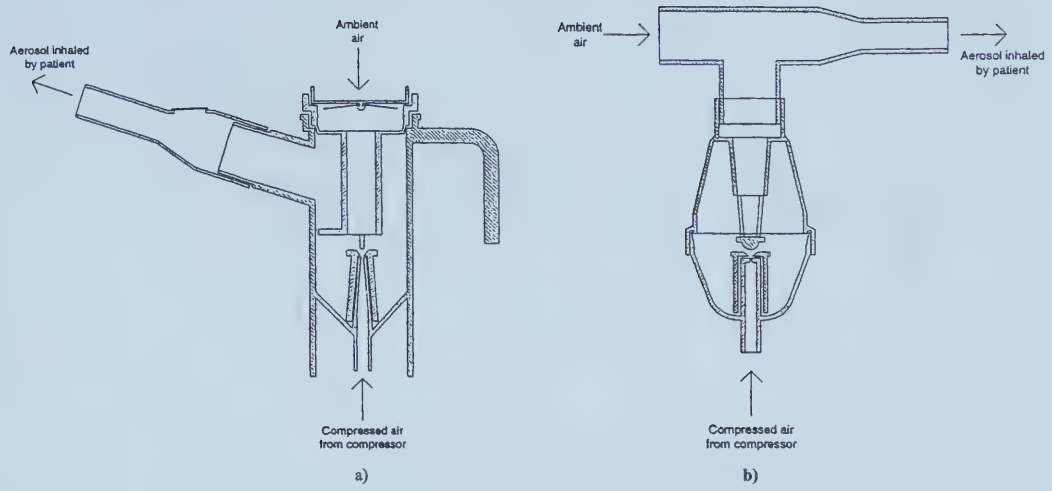

Figure 2.1: Typical a) Vented and b) Unvented Nebulizers [1]

other factors remain constant, we can look at how variations in airflow through a vented jet nebulizer affect aerosol production from the device. The following sections will provide a brief summary of the physics behind aerosol generation in a vented jet nebulizer. The particular nebulizer used in this study, an LC⋆ vented jet nebulizer (Pari GmbH, Starnberg, Germany), is considered in the following sections although the principles discussed are appropriate for vented jet nebulizers in general. A more detailed and exhaustive presentation of the topics summarized in the following sections is given in Finlay [2].

2.3.1 Particle Size

Droplet production in nebulizers occurs due to a high speed air jet shooting up through a column of water. A compressor is used to blow air up though a nozzle (1) (Refer to Figure 2.2 on page 11 throughout). This nozzle creates a low pressure area that draws the nebulizer solution (2) into a small area where it forms a liquid sheath around the air jet (3). It is the instability of this air/water interface that leads to primary droplets being formed and shed from the bulk fluid into the air jet.

The size of the primary droplets can be dependant on many variables including surface tension, density and viscosity of the liquid, compressor flow rate, and density of the gas but generally not on the breathing airflow through the body of the device. These initial particles

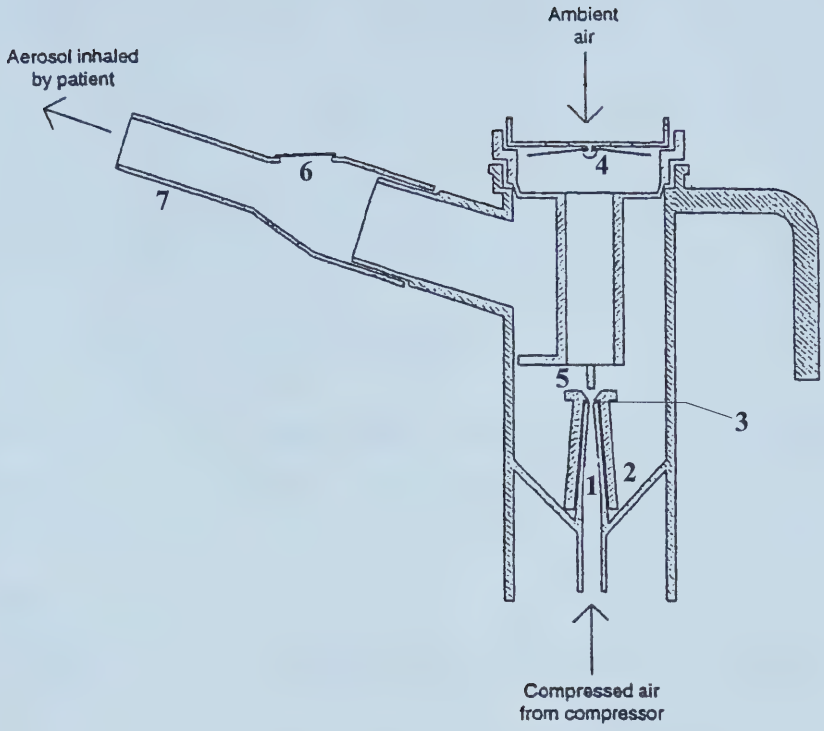

Figure 2.2: Pari LC⋆ Vented Jet Nebulizer used in this study: 1) Venturi nozzle 2) Solution to be nebulized 3) Liquid sheath around air jet 4) Inhale valve 5) Baffles 6) Exhale valve 7) Mouthpiece [1]

are very large, relatively speaking, and are not the final particles that are output from the device. Instead, most of these drops will reconstitute with the bulk fluid in the reservoir to be nebulized again. A small fraction of these primary droplets, however, undergo secondary and tertiary breakup processes which reduce the particles to sizes that have a chance to make it out of the device and it is these breakup processes that can be affected by the breathing airflow through the device.

2.3.1.1 Aerodynamic Loading

At creation, primary droplets can experience large aerodynamic forces due to their considerable relative velocity compared with the air jet. This may act to break up the droplets and depending on the degree of aerodynamic loading, droplets can break up according to different regimes or not break up at all. The classification of the droplet breakup domains can be represented by two nondimensional parameters with the most commonly chosen ones

being the Reynolds and Weber numbers seen in Equations 2.5.

$$a) \quad Re_d = \frac{\rho_d U d}{\mu_d} \qquad b) \quad We_d = \frac{\rho_g U^2 d}{\sigma} \tag{2.5}$$

where Re_d — droplet Reynolds number;
We_d — droplet Weber number;
ρ — density of gas (g) or droplet(d) [kg/m^3];
U — flow velocity [m/s^2];
d — particle diameter [m];
μ_d — droplet fluid viscosity [kg/m·s];
σ — surface tension [N/m];

The breakup domains have been classified empirically in terms of cutoff values for the Weber number. Although there is not complete agreement regarding the specific cutoff values or the nomenclature used to describe the domains, a general regime classification is shown in Table 2.1.

Breakup Regime		Empirical Values	Type of Breakup
1	$We < We_0$	$We < 12$	Below cutoff no breakup occurs
2	$We_0 < We < We_1$	$12 < We < 40 - 100$	Vibrational, bag, bag & stamen
3	$We_1 < We < We_2$	$40 - 100 < We < 350 - 1000$	Sheet stripping
4	$We > We_2$	$We > 350 - 1000$	Catastrophic breakup

Table 2.1: Droplet breakup regimes classified according to drop Weber number (Eq. 2.5b)

Most of this aerodynamic loading, however, is expected to occur very near the nozzle (3) and very soon after the particle is shed from the bulk fluid. As a result, we suspect that variations in breathing airflow drawn through the top valve (4) of a vented nebulizer would not have any effect. The flow velocity found in Equations 2.5 would likely be dominated by the high speed compressor jet component and variations in the breathing flow would be inconsequential at this stage.

2.3.1.2 Baffle Impaction

Droplet breakup also occurs as the result of impaction and splashing on the internal baffles of the device (5). The Weber and Reynolds numbers can be used in a different way (K_c as seen in Equation 2.6) to quantify the likelihood that particles will impact and splash on a baffle and give an indication of the resultant sizes of the drops produced by this process.

$$K_c = \sqrt{We_d Re_d^{1/2}} = \sqrt[4]{\frac{\rho_d^3 d^3 U^5}{\sigma^2 \mu_d}} \tag{2.6}$$

where ρ_d — droplet liquid density [kg/m^3];
d — droplet diameter [m];
U — flow velocity [m/s];
σ — surface tension [N/m];
μ_d — droplet fluid viscosity [kg/m·s];

Again, empirical results have been obtained that attempt to quantify the resultant particle size after a droplet impacts and splashes on a surface [17, 18]. We can extend the conclusions drawn from these studies to the case of particles splashing on the internal baffles of a nebulizer. Examination of droplet splashing on both dry and wet surfaces found a cutoff value for K_c below which droplets will not splash upon impacting. Both studies found that as K_c increases above the cutoff the resultant splashed particles will decrease in size and approach an asymptotic value of 0.06 of their original size (d_i). The empirical results for K_c values and ensuing splashed drop size are shown in Table 2.2.

Dry surface [17]		Wet surface [18]	
K_c	Size	K_c	Size
<57.7	no splash	<324	no splash
130	$0.6d_i$	>324	$0.06d_i$
175	$0.1d_i \rightarrow 0.06d_i$		

Table 2.2: Empirical K_c (Eq. 2.6) values and splashed drop size

In this case, variations in breathing airflow may indeed affect the parameter K_c. As mentioned above, however, the size of the splashed drops quickly approach an asymptotic value of $0.06d_i$. For an LC$\star$ nebulizer the first baffle is very near the nozzle exit and K_c would be of order 1000. As a result all droplets would be expected to splash into drops of size very near the asymptotic value of $0.06d_i$, regardless of breathing airflow variations.

2.3.1.3 Baffle Size Filtering

Internal baffles can also be considered as size filters allowing only particles smaller than a certain size to pass. In the same way that particles inertially impact in the respiratory tract (see section 2.2.2.1 on page 6) particles can only follow the flow around internal baffles up to a certain particle size and fluid velocity. This can be quantified by considering an

approximate particle diameter, d_{50}, that has a 50% chance of impacting on a baffle. An empirical expression for d_{50} is shown in Equation 2.7 [2].

$$d_{50} = \sqrt{\frac{9\mu_g D}{\rho_d U}}/4 \tag{2.7}$$

where d_{50} — 50% cutoff diameter [m];
μ_g — viscosity of air [kg/m·s];
D — characteristic flow diameter [m];
ρ_d — droplet liquid density [kg/m^3];
U — flow velocity [m/s];

It can be shown that virtually all particles exiting the nozzle will impact on the primary baffle and again breathing airflow will have little or no effect. Impaction on secondary baffles, however, could indeed be affected by the breathing airflow since the flow velocity would slow and expand considerably from the narrow jet exiting the nozzle. This could bring variations of d_{50} into the respirable range thus affecting dosages in the lungs. Experimentation is then required since the internal geometries of the device are quite complex and droplet impaction cannot be characterized or predicted precisely.

2.3.2 Output Amounts

The total amount of aerosol output from a vented jet nebulizer generally increases with an increase in inhalation flow rate, hence the alternate terminology: breath enhanced nebulizer. Consequently, variations in breathing flow rate can be expected to alter device output. In addition, aerosol is continually produced during exhalation and lost out of the exit valve (6). Thus, differences in exhalation duration can alter the total amount of aerosol lost to the environment and consequently the total amount delivered to the mouthpiece for inhalation.

2.4 Summary

Drug delivery using vented jet nebulizers can be broken down into two components. First, the actual output of the device, in terms of amount of drug produced and the size distribution of the particles at the exit of the nebulizer. Second, the deposition fate of the resultant particles delivered to the mouth and available for inhalation. Each stage in this process has a dependency on the airflow or breathing pattern implemented. Consequently, this report

will examine the effect of the functional shape of the breathing pattern used in testing vented jet nebulizers. It will attempt to assess its importance in keeping *in vitro* experiments as realistic as possible as well as suggesting a standard for nebulizer bench testing.

Chapter 3

Experimental Design

3.1 Introduction

This research is broken down into three major sections with each ensuing section building on the previous one. The first stage involves the collection of real breathing patterns. Breathing patterns are to be measured for real human subjects while breathing normally and then through a nebulizer. The recorded breathing waveforms will be averaged into a representative waveform for each subject and characterized in terms of common breathing parameters, such as tidal volume, breath frequency and duty cycle. Differences between each individual's nebulizer and normal breathing patterns will be examined and will hopefully corroborate previously published results. Of more interest, however, are differences in the actual functional shape of the breathing waveforms, which to our knowledge has not been examined in detail in this way. The representative waveforms will then be prepared for use in the following phase of the study.

The second stage involves recreating the "real" breathing patterns obtained in the first phase with a mechanical breath simulator. The simulated breaths will be used in a simple but effective *in vitro* bench test setup. This bench test will be used to compare the effect of differences between an individual's nebulizer and non-nebulizer breathing patterns to sine and square wave patterns of equivalent breath parameters. The nebulizer output will be characterized in terms of the particle size distribution and the total amount of drug available for inhalation.

The third stage of this study involves inputting the different breathing patterns combined with the particle size and inhaled amount data obtained from part two into a computer model

designed to predict the regional deposition patterns in the human lung. The computer model is an Eulerian two-way coupled simulation using variable boundary conditions.

As stated before, variation in flow patterns can affect nebulizer drug delivery in two ways. Flow patterns through a vented jet nebulizer can affect the output of the device in terms of amount and particle size distribution of the drug delivered to the mouthpiece for inhalation. Additionally, flow patterns in the respiratory airways have a direct correlation to where particles will end up depositing. Consequently, differences in flow patterns can cause differences in deposition patterns independently from the flow pattern effects on the device. It is hoped that the three stages of this experimental design will allow the significance of breathing pattern differences on vented jet nebulizer drug delivery to be determined and characterized.

3.2 Part I – Collection of Breathing Patterns

The initial stage of this study involved the collection of real breathing patterns from normal healthy individuals [19]. Twelve volunteers with an average age of 24 years were obtained from the University of Alberta student population and given a brief clinical exam. The purpose of the exam was to deem the subjects normal and healthy through a series of standard lung function tests and to screen individuals with evidence of any of the following exclusion criteria: evidence of pulmonary or chronic obstructive airways disease, smoker within three years, asthmatic, woman of childbearing potential, medications likely affecting pulmonary function, or lack of informed consent.

3.2.1 Plethysmograph

A head out plethysmograph was used to sample each person's breathing pattern. The function of the plethysmograph is straightforward and is diagrammed in Figure 3.1. A person sits in the airtight box sealed with a neoprene collar at the neck and simply breathes. Entry into the box is accomplished by removing a side panel and sliding in laterally. The seat is also adjusted to ensure each subject is relaxed and sitting comfortably.

The expansion of the chest and abdomen reduce the volume inside the box resulting in a measurable pressure increase. This pressure change can easily be detected and sampled

by a Validyne pressure transducer (CD15, Validyne Engineering Corp., Northridge, CA, USA) and recordable digital oscilloscope (TDS 410A, Tektronix, Wilsonville, OR, USA) data acquisition system. The output from the Validyne pressure transducer is a voltage vs. time trace which requires postprocessing. An initial pressure/volume calibration is done with the subject holding his breath by injecting a set volume of 1L into the plethysmograph and recording the static voltage change on the Validyne. This is dependent on the residual volume in the box due to size differences among the subjects. It is done immediately before commencing each test to allow for the direct linear conversion from the measured voltage output into the desired lung volume changes.

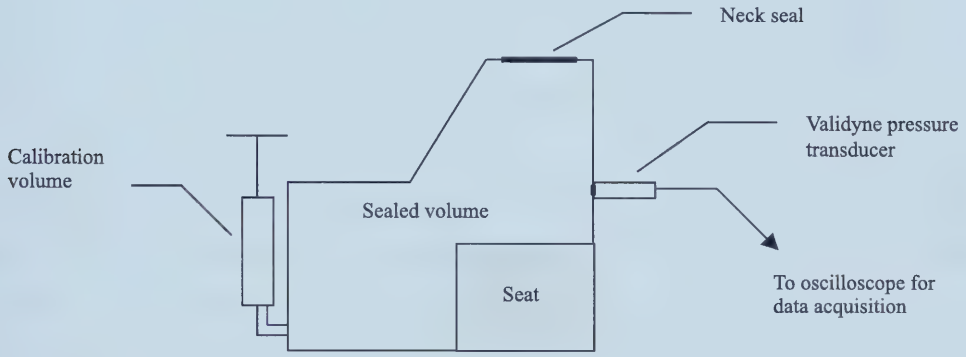

Figure 3.1: Head-out Plethysmograph (side view)

3.2.2 Breath Sampling

The subjects performed two different tests, first breathing normally without any facial apparatus and then breathing through a nebulizer. In either case, they were not aware that the breathing patterns were being measured. In the first test the subjects breathed normally for approximately ten minutes while watching television with the lung volume changes sampled for five minutes in the middle of the test to eliminate start and end effects. The second test involved breathing in saline droplets nebulized using an LC⋆ nebulizer and Turboneb compressor (Pari GmbH, Starnberg, Germany). For each subject, a new nebulizer was charged with 2.5mL of saline solution (0.9% mass concentration of NaCl) and breathing was done using a mouthpiece and noseclips. Each subject was told to breathe normally just as in the previous test until nebulization was complete. End of nebulization was indicated when

aerosol droplet production paused for more than 15 seconds. The nebulization time averaged 6.1 minutes for all the subjects and, again, lung volume measurements were made for five minutes in the middle of the nebulization time.

3.2.3 Postprocessing and Comparison of Breathing Patterns

The measurements made with the Validyne pressure transducer were recorded by an attached oscilloscope. The oscilloscope stores the data in its own unique format which is unreadable by any other software, so it is first necessary to extract the data into a more usable format. After the data is converted, however, it is still a raw voltage vs. time signal. The data then needs to be transformed to a volume vs. time signal by a direct multiplication with the conversion factor obtained from the 1L syringe calibration. Once this conversion is done the data can be stored on a computer and postprocessed as needed.

The five minute volume trace is not very useful in itself. Instead, it is desirable to take an average of all the breaths during the sample time and form a single breathing waveform representative of the particular individual under study. Then the effect of breathing through a nebulizer can be examined directly by comparing standard breathing parameters as well as the functional shape of the waveform.

Prior published results demonstrate that breathing through a nebulizer (or any breathing apparatus such as mouthpiece or facemask) does indeed change a person's breath pattern [20–27]. In general, breathing through a nebulizer tends to increase the tidal volume and lengthen the period while changes to other parameters, such as minute ventilation, show no conclusive trends. Most interesting to us, however, is the effect on the functional shape of the breathing waveform, which has seldom been examined. One study compared measurements taken of the functional shape of subject's breathing patterns initially and 4-5 years later [14], concluding that people maintain a high degree of shape individuality of their breathing pattern despite changes in age, fitness, or smoking habit. But to our knowledge no detailed examination has been done regarding the effect of breathing apparatus on the functional shape of a breath.

To isolate shape effects from effects due to differences in minute ventilation, the average waveforms need to be scaled to normalized values for the standard breath parameters. For

the next part of the analysis, breathing patterns will be considered in sets of four. A sine wave, square wave, normal pattern and nebulizer pattern will be scaled to the average breath parameters for each respective subject. This ensures that the minute ventilation is constant across each set and that the only variation is in the waveshape between the zero crossings of the flow. Finally, the representative scaled breathing patterns must also be output into a form acceptable as input in the computer controlled breath simulator used in part two.

3.3 Part II – *in vitro* Bench Testing

An effort was made to keep the *in vitro* setup as simple as possible. The setup is shown in Figure 3.2 and consists of four parts. 1) The computer controller piston, termed the Happy Breathing Machine or HBM, used to recreate the breathing pattern, 2) the nebulizer under test, 3) the measurement window to allow real time particle sizing using phase Doppler anemometer (PDA) technology, and 4) the collection filter. Each test consisted of running the nebulizer for five minutes, nebulizing 3mL of a 0.9% saline solution while sampling the particle size distribution for 10s at the beginning of each minute.

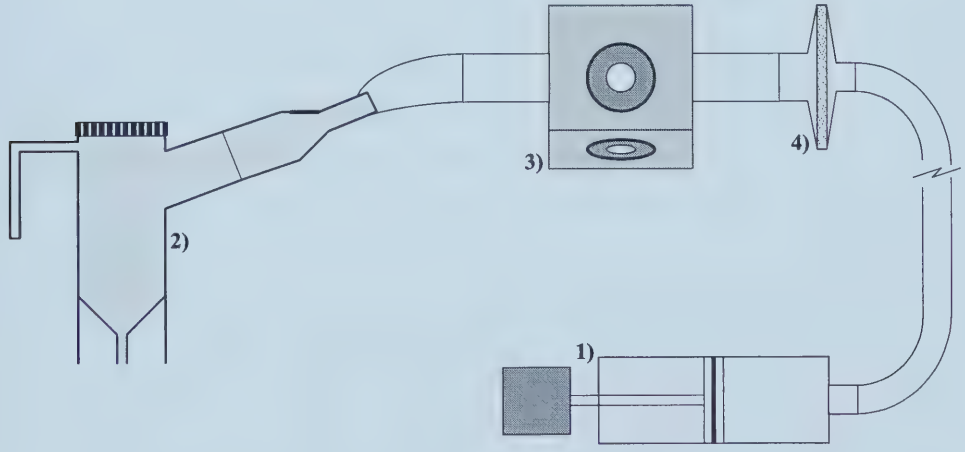

Figure 3.2: Nebulizer Bench Test Setup: 1) HBM breath simulator 2) LC⋆ nebulizer 3) PDA measurement window 4) Collection filter

3.3.1 Vented Jet Nebulizer

The nebulizer chosen for these tests is an LC⋆ vented jet nebulizer (Pari GmbH, Starnberg, Germany). It was chosen because it has been used previously in our lab and is known to

provide reliable and reproducible results. We consider it to be one of the most efficient and effective devices for delivering drug of the appropriate sizes for inhalation [28]. The nebulizer was driven with a DeVilbiss Pulmo-Aide compressor (model 5610C, DeVilbiss Health Care Inc., Missisauga, ON, Canada) operating at 4.6L/min.

3.3.1.1 Nebulization Time

Many researchers commonly signal the end of testing by running nebulizers to dryness. The spitting and sputtering that occurs as a device nears the end of nebulization, however, is random and unpredictable. This is unacceptable when trying to produce a consistent and reproducible bench testing method. As a result, the nebulizers in this test are run for a set amount of time, short of the onset of sputtering.

Since nebulization time to dryness is directly related to the initial fill volume of the nebulizer (i.e. the larger the fill volume the longer nebulization time) a preliminary test was done to quantify this effect and to determine an appropriate fill volume for these tests. Table 3.1 shows nebulization time results for fill volumes of 2.5mL and 3mL inhaled by a symmetrical square wave scaled to the breath parameters resulting in the largest minute ventilation used in this study (i.e. a tidal volume of 0.646L and period of 2.872s). Running this preliminary test at the maximum possible minute ventilation guarantees that all other tests would result in even longer runs. Based on these results, a fill volume of 3mL was chosen for convenience and to ensure that sputtering would not be encountered for a test time of five minutes.

	Nebulization Time (min:s)		
Fill volume (mL)	Test 1	2	Average
2.5	4:28	4:32	4:30
3.0	6:35	6:27	6:31

Table 3.1: Nebulization time for fill volumes of 2.5 and 3mL

3.3.1.2 Assay Method

After test completion, the amount of saline left in the nebulizer is assayed. The residual saline is determined using the mass difference before and after the test and the concentration of the solution left in the cup. All internal surfaces of the nebulizer are repeatedly rinsed with

3mL of water and the concentration of the resultant solution is measured using freezing point osmometry. The concentration is measured using an osmometer (μOsmette 5004, Precision Systems Inc., Natick, MA, USA) which functions by freezing a 50μL sample of the solution and measuring the freezing point depression which varies in proportion to the amount of solute present.

3.3.2 Phase Doppler Anemometry

3.3.2.1 Theory of Doppler Anemometry function

A phase Doppler anemometer system (Dantec Electronics Inc., Mahwah, NJ, USA) is used to provide a real time measurement of the particle size distribution of the aerosol exiting the nebulizer. Phase Doppler laser anemometry is a 2D extension of 1D laser Doppler anemometry. In both cases, incident light scattered by a particle is radiated through the receiving optics, detected by photomultipliers, and analyzed and interpreted by a signal processing unit.

Laser anemometry, in general, consists of a laser emitting into a transmitting optics assembly that splits the laser into two congruent beams. The two laser beams are then focused through a lens with the intersection point designating the measurement volume. The measurement volume seen in Figure 3.3 is defined as the 3D volume from -a to a, -b to b, and -c to c along the y axis perpendicular to the page. It is formed by the two cylindrical beams of diameter d intersecting at an acute angle θ. The intersection of the beams generate an interference fringe pattern with fringe spacing dependent on the light frequency and intersection angle. As a clear spherical particle passes through the measurement volume, light will be refracted as seen in Figure 3.4.

The system needs to be setup and configured depending on which scattering mode is to be examined. For our case of water droplets in air, the strongest signal can be detected as first order refraction at Brewster's angle of 73.7°. This optimal angle eliminates reflection for an incident beam polarized parallel to the scattering plane and is dependant on the ratio of the refractive indices of the two mediums. Incidentally, a signal can be detected at angles off of the ideal but the signal to noise ratio diminishes rapidly the farther the receiver is from the optimal angle. The usefulness of this fact will be seen during the validation of the

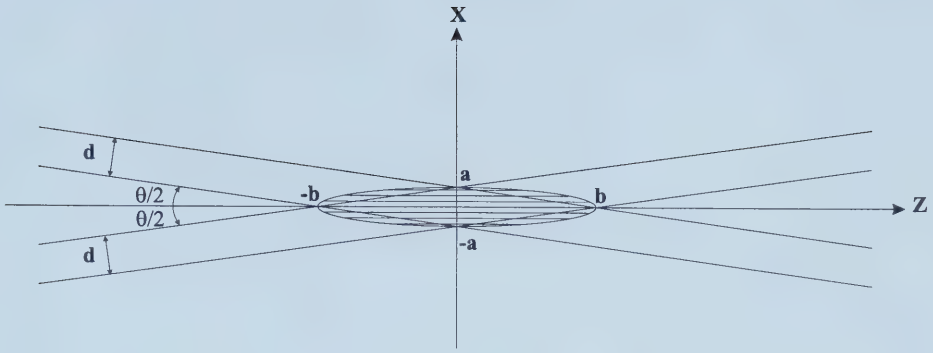

Figure 3.3: PDA Measurement Volume: d – laser beam diameter, θ – beam crossing angle, a, b – measurement volume dimensions

PDA system found in section 4.4.

In the case of 1D laser anemometry, the refracted fringe pattern is detected by a single stationary photomultiplier in the receiving optics as a light source pulsing at the Doppler frequency. The velocity of the particle perpendicular to the fringe plane as it transits across the measurement volume can be determined for a known fringe spacing from this Doppler frequency.

The extension to a PDA system lies with the addition of a second photodetector. As light transits through the receiving optics, it will travel different optical path lengths to each photodetector. This dissimilar optical path length creates a detectable phase difference in the received light which varies with the effective focal length of the droplet which, for spherical droplets, is proportional to the drop diameter.

As is described above, however, the system would contain ambiguity in both the velocity and drop diameter. The magnitude of the Doppler frequency does not, by itself, contain any information as to the velocity direction. To alleviate this, a frequency shift is introduced by a Bragg cell into one of the incident beams. This causes the fringe pattern to move at a set velocity within the measurement volume. Now, the detected light modulation will be centered around the shift frequency with greater frequencies indicating one direction and smaller frequencies indicating the other. There is also an ambiguity in the detected particle size in a two detector configuration, since only phase angles from zero to 2π are unique. Uncertainty in the particle size will occur as the detected phase difference wraps around

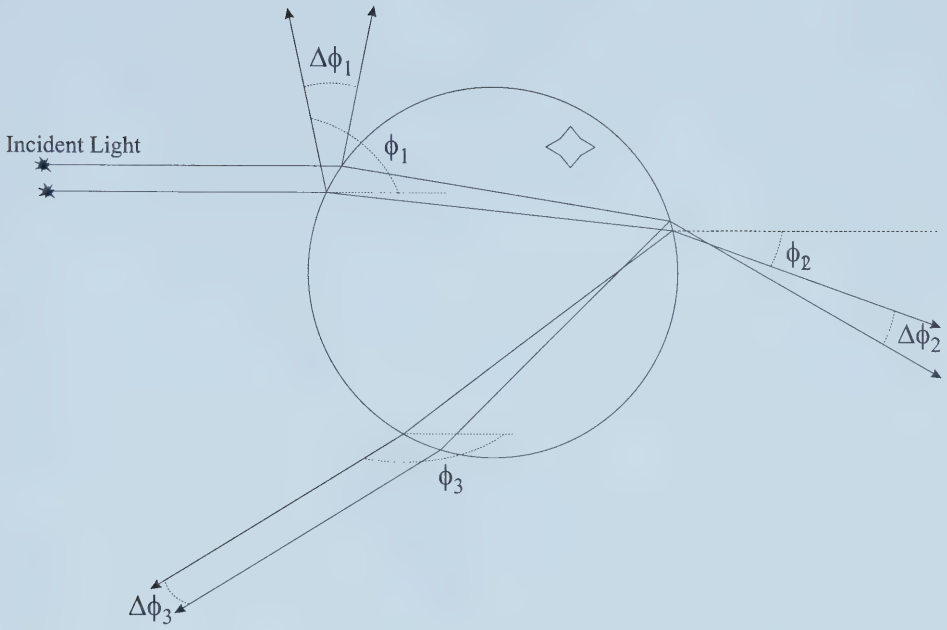

Figure 3.4: Principal scattering modes used by PDA for light refracting through a clear spherical droplet in air: Reflection (ϕ_1), first order refraction (ϕ_2), and second order refraction (ϕ_3)

2π. The addition of a third photodetector at a different optical path length resolves this problem. In this way, the phase differences between two pairs of photodetectors can be compared to define an unambiguous particle size.

3.3.2.2 Nebulizer Particle Size Measurements

The measurement window was designed to be inserted between the mouthpiece of the device and the collection filter. In adding the inline measurement window it is important to keep the system connection volume minimized. The size of the connection volume (consisting in this case of connection tubing, the measurement window volume, and the filter dead space) in this type of measurement system has been shown to affect test results, especially for pediatric type flow patterns where the tidal volume approaches the magnitude of the connection volume [8, 9, 22, 28]. As a result, the connecting tubes are kept as short as possible and the entry and exit to the measurement window are smoothly tapered to and from the smaller diameter cross-section inside the window.

An expanded view of the measurement window is shown in Figure 3.5. The entry and exit glass are designed to be perpendicular to the transmitted and refracted light. As stated previously, the refraction angle is determined for the particular particle/medium scattering combination, in this case, water droplets in air. Thus, the exit glass is positioned at an angle of 73.7° from the entry glass.

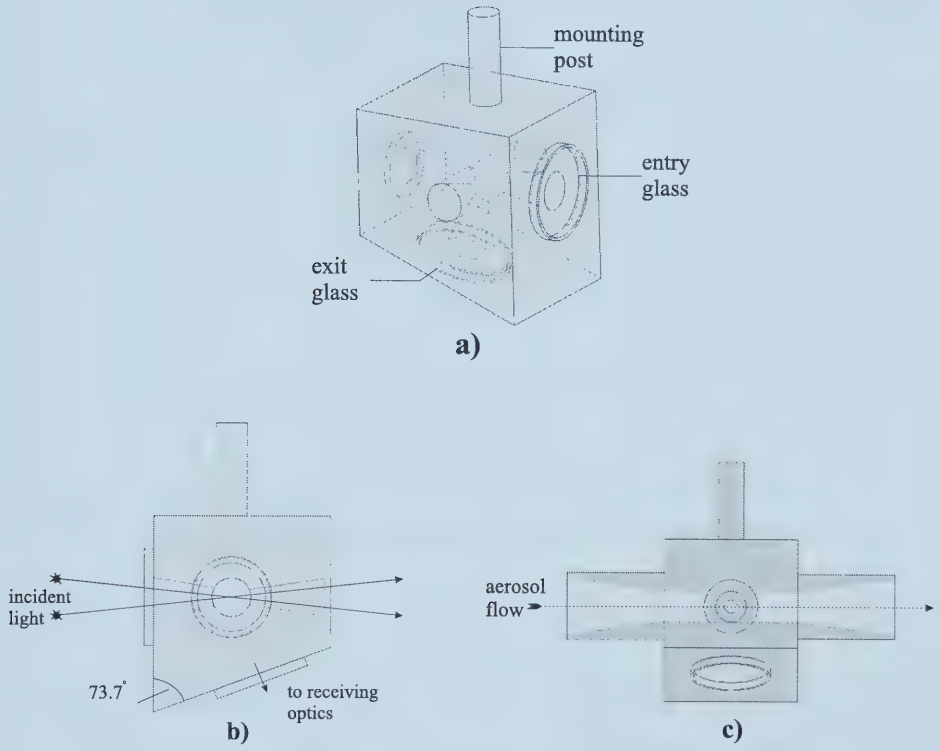

Figure 3.5: PDA measurement window designed for refraction of water droplets in air. a) Internal view b) Side view c) Rear view

The system is controlled with a computer running Dantec SIZEware software (version 2.1). The software and signal processor perform the necessary calculations and display the particle size and velocity online in real time. For each five minute test, however, size data is sampled for 10 seconds at the beginning of each minute and saved to data files. So for a total of six ten second samples, the actual length of the test is five minutes and ten seconds. The user then has the option of analyzing the data within SIZEware or exporting the data

in text file format for later analysis.

3.3.3 Collection Filter

The filter used in the tests are low deadspace Respirgard II hydrophobic anti-viral filters (No. 303, Marquest Medical Products, Englewood, CO, USA) that effectively screen out aqueous particles $>0.3\mu$m with a >99.9% efficiency. After each test, the filter is assayed by rinsing with 3mL of water, massing the amount of matter on the filter, mixing for 45 seconds on a vibrating platform (Type 37600 Mixer, Thermolyne, Dubuque, IA, USA) and measuring the solution concentration using freezing point osmometry.

3.3.4 Happy Breathing Machine (HBM)

The HBM is a cylinder and piston driven by a precise stepper motor controlled by a computer. The controlling software provides the user with two options for creating flow patterns. It allows the user to create a square wave flow pattern of defined tidal volume, period, and duty cycle or an arbitrary flow pattern defined by an input file. The arbitrary flow pattern option was used to generate the normal, nebulizer, and sine breathing patterns. The HBM can continuously repeat single period flow patterns but cannot follow an arbitrary oscillating flow pattern thus necessitating the formation of representative average waveforms.

3.4 Part III – Computer Deposition Modelling

The final stage of this study involved using the results from the previous two stages as inputs into a new particle deposition model in development in our lab called TechAero (*Truly Eulerian Code for simulation of Hygroscopic AEROsols* written by Carlos F. Lange). TechAero uses an Eulerian viewpoint to numerically simulate the transport and deposition of hygroscopic aerosols in the human lung. It has the ability to solve for the fully two-way coupled heat and mass transfer between the continuous phase and the droplet phase as well as the resultant particle deposition probabilities. The droplet phase is represented by three dimensions: the distance from the beginning of the mouthpiece (x), the particle radius (R), and the mass of solute in a drop (m_1).

This new deposition model is unique for several reasons and is described more fully in Lange & Finlay [29]. The Eulerian implementation is an advancement over Lagrangian

models that do not allow for time dependant boundary conditions, including RegDep, the deposition code currently in use in the lab. It is precisely this difference that enables the simulation of the variable breathing patterns central to this research. TechAero is also an improvement over existing Eulerian models, primarily designed for monodisperse aerosols of constant size, that handle the particle phase as a second continuous phase (a multicontinua approach) [30]. These earlier models could be modified to allow for polydisperse aerosols, however, the discrete nature of the size classes does not allow for the distinction of particles of the same size with different solute concentrations resulting from diffusion or recirculating flow.

For this study, however, a major simplification in the TechAero model is possible. The aerosol generated in a Pari LC⋆ saturates the air passing through. This results in an isotonic aerosol entering the mouth at ~99%RH. As a result, the inhaled droplets can be expected to undergo very little hygroscopic size changes and the solute concentration within each drop will remain virtually constant [31]. In effect, this allows the problem to be reduced to two dimensions (x and R) by considering the aerosol as a single substance.

3.4.1 Summary of the TechAero Algorithm

3.4.1.1 Lung Model

Similar to other deposition models, the lung is described as a one-dimensional series of tubes of constant cross-sections. All quantities of interest are averaged over the cross-section for each generation. The model used is a hybrid of two models presented in the literature. The lung is corrected to a volume of 3050cc with the trachea (generation 3) to generation 17 taken from Phillips et al. [32, 33], and generations 18 to 26 taken from Haefeli-Bleuer & Weibel [34]. The actual input file containing the geometry of each lung generation in the model can be found in Figure A.1.

3.4.1.2 Particle Concentration

As mentioned above, TechAero would normally solve the four balance equations for particle concentration, particle enthalpy, vapour concentration and air enthalpy in the continuous phase. In this study, however, the particles are assumed to be stable upon exit from the nebulizer and since no mass transfer will then occur between the particle and continuous

phase, only Equation 3.1 concerned with particle concentration needs to be considered. This reduces the problem domain from three dimensions (x, R, m_1) to two (x, R) by removing the terms containing $\dot{m}_1$ and $\dot{R}$ and greatly reduces the memory demand and computation time.

$$\frac{\partial(nA)}{\partial t} + U\frac{\partial(nA)}{\partial x} + \dot{R}\frac{\partial(nA)}{\partial R} + \dot{m}_1\frac{\partial(nA)}{\partial m_1} = \frac{\partial}{\partial x}\left\{D\frac{\partial(nA)}{\partial x}\right\} + \dot{n}_{dep}A \tag{3.1}$$

where n — particle count distribution;
A — cross-sectional area [m^2];
U — average velocity [m/s];
R — particle radius [m];
m_1 — mass of solute in each particle [kg];
D — effective axial diffusivity [m^2/s];
$\dot{n}_{dep}$ — particle deposition rate [s^{-1}];

The strongly implicit iterative process of Stone [35] is used to solve the discretized system of equations for the particle concentration in every grid cell in the domain for each time step, Δt. The source term $\dot{n}_{dep}A$, accounts for the removal of particles by deposition. The output of interest, however, is the calculated drug dosage to each lung region (extrathoracic, tracheo-bronchial, and alveolar), obtained by the integration of the deposition rate in time.

3.4.1.3 Particle Deposition

The primary deposition mechanisms of particles in the lung were described in section 2.2.2 beginning on page 6. The actual numerical implementation of those processes is described here.

The extrathoracic region is considered as a single unit and the dosage prediction is made based on empirical models presented in ICRP [36]. The expressions describing deposition probability in the oropharynx and larynx due to impaction/sedimentation (P_{IS}) and diffusion (P_D) are given in Equations 3.2 and 3.3 respectively. The total deposition (P_{ET}) in this region is given in Equation 3.4.

$$P_{IS} = 1 - \frac{1}{1.1 * 10^{-4}(d_a^2 Q^{0.6} V_{in}^{-0.2})^{1.4} + 1} \tag{3.2}$$

$$P_D = 1 - e^{-9\sqrt{D}Q^{-1/8}} \tag{3.3}$$

where d_a — particle aerodynamic diameter;
Q — flow rate [m^3/s];
V_{in} — inhalation volume [m^3];
D — Brownian diffusivity [m^2/s];

$$P_{ET} = 1 - (1 - P_{IS})(1 - P_D) \tag{3.4}$$

The following expressions calculate the deposition probabilities in the lung. These expressions are used in all generations from the trachea (generation 3) to generation 26. The only exception is that no sedimentation occurs in the trachea.

Impaction – The probability for deposition by impaction in a given generation is taken from Chan & Lippmann [37] and is shown in Equation 3.5.

$$P_{(I-gen)}(Stk) = 1.606Stk + 0.0023 \tag{3.5}$$

where Stk — Stokes number as defined in section 2.2.2.1;

Sedimentation – The probability for deposition by sedimentation in a particular generation is an analytical approximation taken from Pich [38] with a correction added for a network of randomly oriented tubes from Heyder & Gebhart [39]. As discussed in section 2.2.2.2, the calculation begins with the settling velocity for a particle which is used to determine a dimensionless sedimentation parameter, ϵ. The deposition probability as a function of the sedimentation parameter, ϵ, is shown in Equation 3.6.

$$P_{(S-gen)}(\epsilon) = 2/\pi((2\epsilon - \epsilon^{1/3})\sqrt{(1 - \epsilon^{2/3})} + \arcsin(\epsilon^{1/3})) \tag{3.6}$$

where ϵ — sedimentation parameter as defined in section 2.2.2.2;

Diffusion – Two analytical approximations are used to determine the probability of deposition by diffusion depending on the magnitude of the diffusion parameter (see section 2.2.2.3). The first expression shown in Equation 3.7 is taken from Ingham [40] and is used for h>0.05. The second expression shown in Equation 3.8 is taken from Gormley &

Kennedy [41] and is used for h<0.05. The selection of h=0.05 as the transition point was not arbitrary but is the value at which the two functions intersect.

$$P_{(D-gen)}(h) = 1 - 0.819e^{-14.63h} - 0.097e^{-89.22h} - 0.0325e^{-228h} - 0.0509e^{-125.9h^{2/3}} \quad \text{for h} > 0.05 \tag{3.7}$$

$$P_{(D-gen)}(h) = 6.41h^{2/3} - 4.8h - 1.123h^{4/3} \quad \text{for h} < 0.05 \tag{3.8}$$

where h — diffusion parameter as defined in section 2.2.2.3;

Total Deposition – The deposition probabilities described in the preceding section are determined from the perspective of each lung generation. To convert the probabilities to the Eulerian viewpoint valid for each cell in the grid the transformation shown in Equation 3.9 is made in each case.

$$P_{(X-cell)} = \frac{P_{(X-gen)}\Delta t}{T_{reside}(1 - P_{(X-gen)}L_{fraction})} \tag{3.9}$$

where X — deposition mechanism – Impaction, Sedimentation, or Diffusion;
$P_{(X-gen)}$ — generational deposition probability for mechanism X;
Δt — solution time step;
T_{reside} — theoretical residence time in generation, $\frac{L_{gen}}{U}$;
$L_{fraction}$ — current fractional distance in a generation;

Once this transformation is accomplished the independent deposition probabilities are combined as shown in Equation 3.10.

$$P_{(Tot-cell)} = 1 - (1 - P_{(I-cell)})(1 - P_{(S-cell)})(1 - P_{(D-cell)}) \tag{3.10}$$

3.4.2 TechAero Usage

3.4.2.1 Input

Appropriate input values for grid size in both the x and R directions, the duration of the time step (Δt), and the convergence tolerance were determined through preliminary testing and validation of the code. Using 200 grid points in the x direction and 50 in the R direction,

a Δt of 10^{-4}, and a convergence tolerance of 10^{-5} was sufficient to minimize computation time without sacrificing accuracy. The mouthpiece dimensions, ambient conditions, and particle size domain are common for all tests. An example of the input file used can be found in Figure A.2.

The variable breaths to be tested are input as data files. A segment of an example breath file showing the format of the file is shown in Figure A.3. The square waveform, however, is an exception and is defined within the input file rather than an external breath file. The particle size distribution parameters (MMD and GSD) as well as the particle production rate need to be specified based on the bench test results from part two of the study.

3.4.2.2 Output

The following files are output by TechAero: *grid.out, locdep.out, gendep.out, and regdep.out.* Examples of all these output files are shown in Figures A.4 to A.7. The solution grids that were used for the x, R, and m_1 dimensions are printed in *grid.out* while dosage amounts for each specific cell and for each generation are presented in *locdep.out* and *gendep.out* respectively. While these output files are useful for debugging or for more detailed examinations of regional deposition, the primary output of interest is contained in the file *regdep.out.*

Regdep.out summarizes the input parameters in three sections: Computation Parameters, Ambient and Physiological Data, and Aerosol Data. The final category presents the regional deposition results for total, extrathoracic, tracheo-bronchial, and alveolar dosage as an absolute amount and as a percentage. Since all other parameters were kept constant, any difference in the regional deposition percentages between tests could only be the result of the varying breath patterns used.

Chapter 4

Validation of Test Methods

4.1 Introduction

This chapter presents the methods and results that were used to validate each aspect of the study. Both the experimental methods and the analysis techniques used in each stage of this research were scrutinized.

4.2 Plethysmograph

Head-out plethysmography is one of the better methods for measuring ventilation in humans due to its simplicity and non-invasive nature. Although not convenient for breath monitoring in a clinical situation or during prolonged activity, it is direct and accurate [42]. Since compression of the chest and abdomen tissues are negligible, there is a direct correlation between volume inhaled and the volume change inside the box.

4.3 Reproducibility of Breathing Patterns

4.3.1 Procedure

The degree of accuracy with which the HBM can regenerate the representative breathing patterns was checked with an inline flowmeter. A sensitive pneumotach (4719 series, Hans Rudolph Inc., Kansas City, MO, USA) consisting of two pressure taps on either side of a screen was inserted into the flow. The pressure differential across the screen is linearly proportional to the flow rate through the device. The pneumotach used is intended for fully developed laminar flow and has a range of 0-100L/min corresponding to a pressure drop of 0-10mmH_2O across the obstruction. A sensitive Validyne pressure transducer (DP45-16,

Validyne Engineering Corp., Northridge, CA, USA) with a full scale range of 0-36mmH_2O was used to detect the slight pressure differential.

The voltage output from the Validyne was detected and sampled at 100Hz using a computer running Dasylab software (version 5, Datalog GmbH, Germany). A program was written in Dasylab that would take the voltage measurement from the Validyne, convert it to a pressure and then convert the pressure into a measured flow rate through the pneumotach. The conversion factors were determined by an initial calibration using a graduated water column to calibrate the Validyne and a dry gas meter (DTM115, Singer American Meter Division) to calibrate the pneumotach. The program displays the flow rate on screen in real time using an instantaneous digital display and a progressive flow vs. time plot. The user also has the option to write the measurements to disk. The flow rate measurements recorded using this system were then compared directly to the original waveforms to check if the HBM precisely recreates the input waveforms.

4.3.2 Results

These preliminary tests showed that the HBM did not recreate the breathing patterns identically but that the level of error introduced is deemed acceptable. Inclusion of the additional flow from the nebulizer compressor was inconsequential. In virtually all cases, the measured flow rate was slightly lower than the nominal value. Amplitude errors were typically in the range 2–3% with a few in the range 3–5%. The breath periods compared favorably with typical differences less than 1.5%. Most importantly, even with the amplitude and period errors, the recreated breathing pattern followed the functional shape of the nominal signal quite well.

The exception was with square wave patterns. In general, the average amplitude was very near nominal and within acceptable errors. The transient overshoot, expected when simulating an ideal square wave, was quite large (averaging ~10%) but died away quickly. The error in the period, however, which ranged from ~4–8%, cannot be considered negligible. Figure 4.1 displays breathing pattern comparisons for typical nebulizer, normal, sine, and square waveforms.

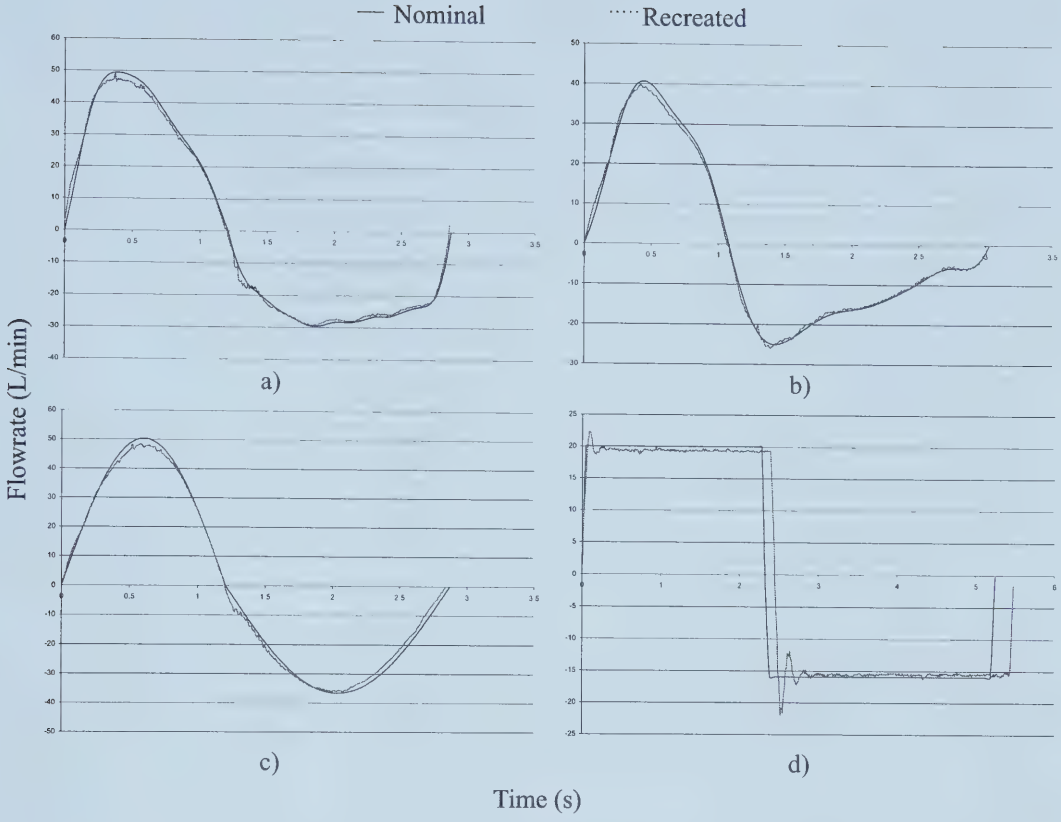

Figure 4.1: Validation of recreated breathing patterns. Typical a) Nebulizer, b) Normal, c) Sine, and d) Square waveforms

4.4 PDA Particle Size Measurements

4.4.1 Procedure

The PDA system was setup and used according to the procedure outlined in the instrument manuals. The device was tested by nebulizing polystyrene microspheres (Bangs Laboratories Inc., Fishers, IN, USA) to confirm the stated accuracy. Monodisperse polystyrene microspheres of sizes 2.5, 3.69, 4.2, and 6.0μm were used to coordinate with the expected size range output of the LC$\star$ nebulizers. The setup for these validation tests was similar to the bench test setup used for the breathing pattern experiments except for a 6' length of tube inserted between the nebulizer and the measurement window. This long tube allows the solvent time to evaporate off the particles since any solvent left on the microspheres as they pass through the measurement window would distort the size measurement to larger

apparent sizes. Preliminary tests were done to determine an appropriate solvent and tube length as well as suitable dilution ratio.

The microspheres were stored in a highly concentrated mixture of solids in water, but were diluted with methanol instead. Water evaporates much less easily and would require a much longer tube to guarantee that the particles are fully dry when reaching the window.

The dilution factor is determined to ensure that, upon nebulization, each droplet of solvent will contain a single microsphere [43]. Droplets containing multiple spheres may lead to unacceptable multi-particle aggregates once the solvent evaporates off. Conversely, if the microsphere number concentration is too small then there may not be enough particles getting to the PDA measurement volume to provide a sufficient measurement data rate. Since the microspheres are produced for a volume concentration of 10% solids, a linear decrease in particle size increases the number concentration cubically.

As discussed in section 3.3.2.1, the optimal signal strength is obtained at Brewster's angle which is defined for a given particle/medium combination. A signal can still be used at angles moving off this optimum angle if a lower signal to noise ratio can be tolerated. This fact allowed the PDA system to be validated in the exact setup used in the bench testing. Even though the measurement window was designed for angles corresponding to Brewster's angle for water droplets in air (73.7°), a strong enough signal can still be detected for polystyrene microspheres in air which have a Brewster's angle of 64.3°.

4.4.2 Results

The stated accuracy of the Dantec PDA system for the diameter measurements used in this study is ±4%. The manufacturer of the microspheres specified them to be monodisperse with a tolerance defined in terms of standard deviation of the mean. To confirm this stated accuracy, the microspheres were viewed under an electron microscope and many spheres were measured manually. Both these values were compared to the measured values obtained by the PDA system as seen in Table 4.1. The measured values are the average of 3-5 tests performed for each case.

The calibration microspheres were accurately measured within the instruments specified error compared to the diameters measured directly with the microscope. Compared to the

Nominal $\pm\sigma$ (μm)	Microscope (μm)	Measured by PDA $\pm\sigma$ (μm)
2.5 $\pm$ 0.03	2.47 – 2.75	2.76 $\pm$ 0.08
3.69 $\pm$ 0.05	?	3.65 $\pm$ 0.05
4.2 $\pm$ 0.04	3.9 – 4.1	4.01 $\pm$ 0.07
6.0 $\pm$ 0.03	5.6 – 5.8	5.69 $\pm$ 0.09

Table 4.1: Calibration of PDA system using monodisperse polystyrene microspheres

other measurements which agree very well with the directly measured results, however, the measurements for the 2.5μm particles appear to be slightly too large. This may be due to the difficulty in preventing multi-particle aggregates from forming and passing through the measurement volume. The maximum dilution that could be used for the increasingly smaller particles was limited by the maximum volume of solution that can be placed in the nebulizer cup. Even though the size difference between the 2.5μm and 6μm particles is only a factor of 2.4, the undiluted number concentration for the 2.5μm particles is $\sim$14 times larger than the number concentration for the 6.0μm particles. It is not possible, however, to dilute the smaller particles with 14 times more solution. As a result, a trade-off to slight oversizing was required to enable measurements at the 2.5μm size. If these aggregates are present then the size distribution would spread apart from the tight peak expected for a monodisperse aerosol. This was observed as the distribution for the 2.5μm particles was indeed wider than that for the other sizes.

Another test which is commonly employed by researchers in other fields to validate particle measurement systems is to measure a multi-mode aerosol consisting of a combination of all the particles validated independently. Unfortunately, this was not possible in our case due to the small size range of interest. Attempts to measure an aerosol consisting of 2.5, 3.69, 4.2, and 6.0μm particles resulted in a measured size distribution smearing from 2.5μm to over 6μm with no distinguishable modes.

4.5 Saline Assay and Filter Extraction

4.5.1 Procedure

The accuracy of the filter extraction is difficult to validate precisely. The validation procedure is simple, involving injecting a known amount of saline onto the filter and then extracting it using the standard method used in the breathing pattern bench testing (see

section 3.3.1.2). Unfortunately, it is impossible to use an aerosol, as is done in the testing, to apply the known amount. Instead, an exact amount of saline solution pipetted directly onto the filter was used as the standard. Volumes of 0.10, 0.15, 0.25, 0.35, 0.50, 0.60, 0.75, 0.85 and 1.0mL were chosen to completely cover the range expected during testing.

4.5.2 Results

The validation of the filter extraction is displayed in terms of mass of saline on the filter in Table 4.2. It is clear that an extraction error is present and must be accounted for. The error tends to grow with decreasing initial amounts. Additional validation tests above 1mg, however, revealed that the error is virtually negligible above this amount. As a result, a piecewise continuous correction can be implemented.

Measured (mg)	Initial (mg)	Absolute Error (mg)	Relative Error (%)
0.000	0.048	0.048	100
0.059	0.099	0.040	40.4
0.099	0.148	0.049	33.3
0.104	0.149	0.045	30.2
0.220	0.248	0.028	11.3
0.324	0.346	0.022	6.4
0.326	0.349	0.023	6.5
0.485	0.498	0.013	2.6
0.599	0.600	0.001	0.1
0.742	0.754	0.012	1.6
0.832	0.848	0.016	1.9
1.005	0.993	-0.012	-1.2

Table 4.2: Validation of filter extraction error

As shown in Figure 4.2, a linear correction works well. Below 1mg, the measured amount of saline extracted from the filter can be adjusted using Equation 4.1. Above 1mg, no adjustment is needed.

$$m_{corrected} = 0.95 m_{measured} + 0.0442 \tag{4.1}$$

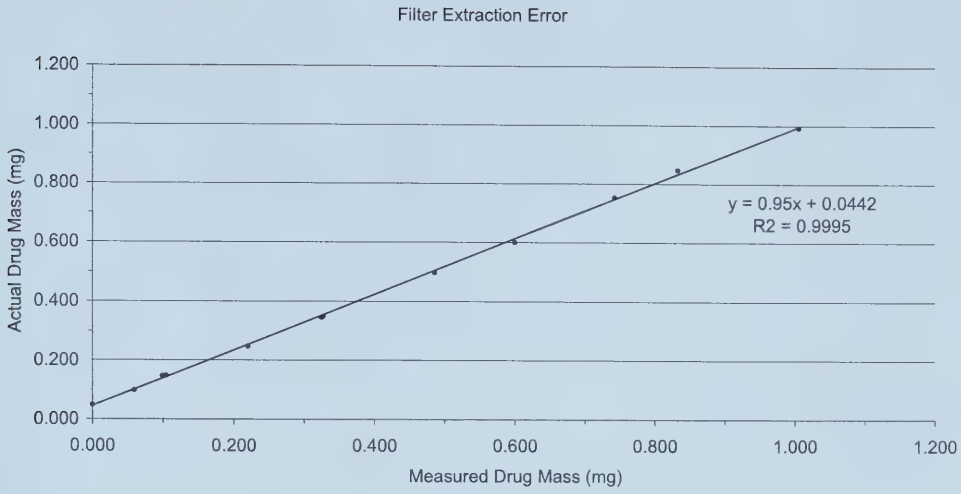

Figure 4.2: Correction of Filter Extraction Errors

4.6 Deposition Model

Before TechAero could be trusted to compare the effect of breath differences on regional drug deposition, it needed to be validated against both theory and previous deposition model and *in vivo* results. Theoretical results describing aerosol deposition by sedimentation from constant flow in a straight circular tube presented by Heyder and Gebhart [39] allowed for specific testing of the implementation of the sedimentation theory. Data compiled in Stapleton [1] allowed for comparison to the Lagrangian deposition model, RegDep, currently in use in the lab as well as a compilation of published *in vivo* data.

4.6.1 Straight Tube Sedimentation

For a given sedimentation parameter, ϵ or T (Equation 4.2), the probability that a particle will deposit via sedimentation in a horizontally oriented straight circular tube is given in Equation 4.3 [39]. Conversely, the probability that a particle will penetrate to the end of the tube is given in Equation 4.4.

$$\epsilon = 3T/4 = (3v_s L_{tube})/(4D_{tube}\overline{U}) \tag{4.2}$$

$$D_s(\epsilon) = 2/\pi((2\epsilon - \epsilon^{1/3})\sqrt{(1-\epsilon^{2/3})} + \arcsin(\epsilon^{1/3})) \tag{4.3}$$

$$P_s(\epsilon) = 1 - 2/\pi((2\epsilon - \epsilon^{1/3})\sqrt{(1-\epsilon^{2/3})} + \arcsin(\epsilon^{1/3})) = 1 - D_s(\epsilon) \tag{4.4}$$

where ϵ — sedimentation parameter;
D_s — sedimentation deposition probability;
P_s — sedimentation penetration probability;
v_s — particle settling velocity $[m/s]$;
L_{tube} — length of tube or generation $[m]$;
D_{tube} — diameter of tube or generation $[m]$;
$\overline{U}$ — average flow velocity in tube $[m/s]$;

Figure 4.3 shows the penetration probability plotted as a function of the sedimentation parameter T. It is clear from Equations 4.4 and Figure 4.3 that as ϵ approaches 1 or T approaches 4/3 asymptotically the penetration fraction drops to zero. This value of the sedimentation parameter above which all particles will deposit in the tube defines the limiting trajectory.

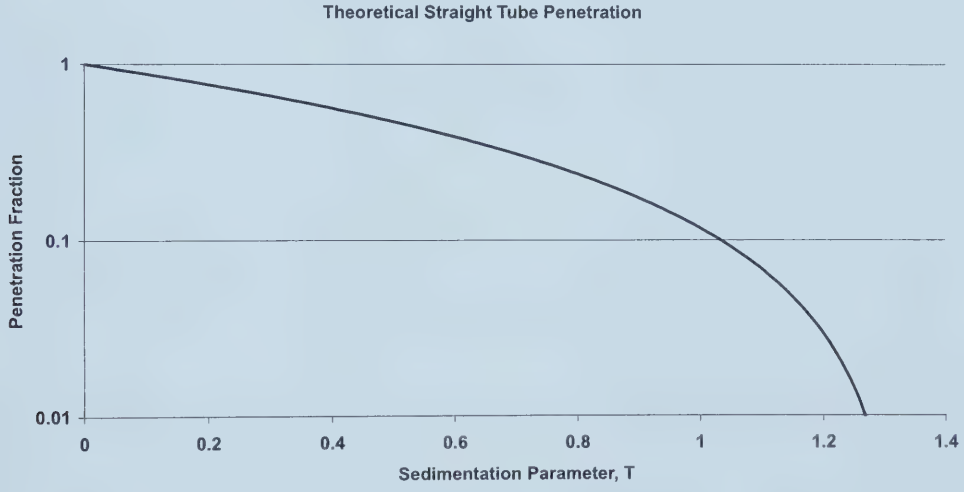

Figure 4.3: Theoretical penetration probability due to sedimentation as a function of sedimentation parameter T

TechAero was run with a monodisperse aerosol in a constant and continuous flow through a straight tube of user-defined dimensions. It was run for many combinations of flow rate, tube geometry, and particle size to cover the full range of the sedimentation parameter $0<T<4/3$, from total penetration to total deposition.

The penetration fraction should depend only on the dimensionless sedimentation parameter and have no additional dependencies on the constituent variables that make up this

parameter. As seen in Figure 4.4, however, results from TechAero displayed an additional dependency on the particle size that was used. As the particle size increased, the total deposition decreased. Regardless of the flow rate and tube geometry, a unique penetration fraction curve was defined for each particle size. Additionally, the limiting trajectory tail-off was not observed as expected at T=4/3. Figure 4.5 shows one case using 3.5μm particles. Instead of representing the limiting trajectory, the observed tail-off defines the aerosol concentration wavefront. When plotted after continuous flow for 30, 40, and 50s, the progression of the wavefront becomes clear. No limiting trajectory is observed, instead, the aerosol is simply being pushed further down the tube.

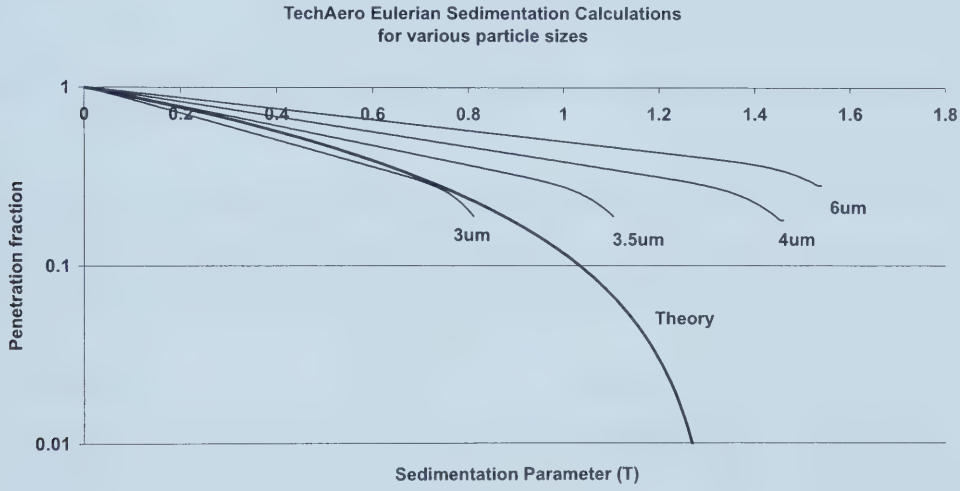

Figure 4.4: Penetration probability from TechAero due to sedimentation for a monodisperse aerosol in a straight circular tube

Both of the above results can be explained by an assumption and known limitation of the TechAero Eulerian code. In implementing the Eulerian calculations, the domain (lung model or straight tube in this case) is discretized into cells for which the aerosol particle concentration is calculated for each time step. At the beginning of each cell, the aerosol is considered homogeneous and well-mixed across the entire cross-section, however, this assumption is not rigorously true throughout the entire domain. In reality the aerosol is not continuously remixed throughout each generation but is continuously settling towards the bottom of the tube. It may be remixed due to secondary flows at bifurcations but not several times within a single generation. This can be visualized as in Figure 4.6 which shows

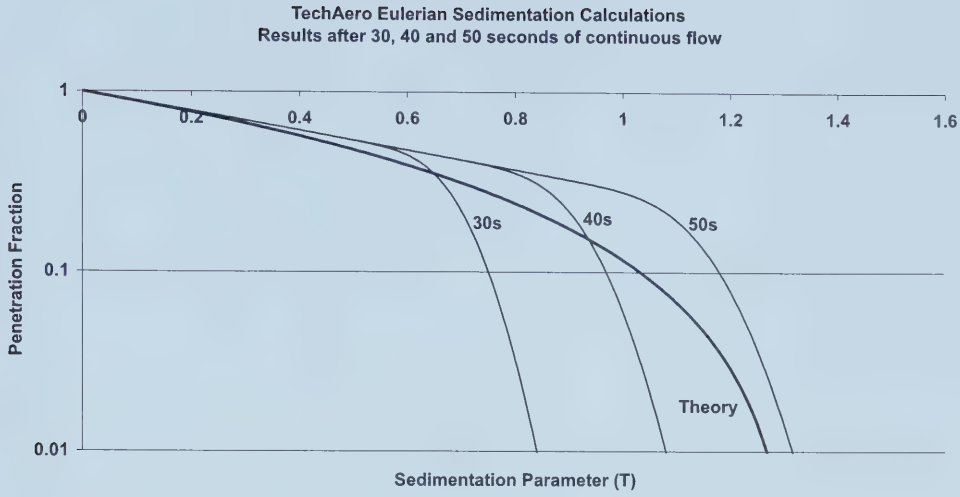

Figure 4.5: Expected limiting trajectory for monodisperse aerosol in straight circular tube at $T = 4/3$

how the particles are assumed to settle within each generation. Thus particles which would be approaching the bottom of the tube are redistributed across the full cross-section. As a result, the particle concentration will continue to approach but will never reach zero.

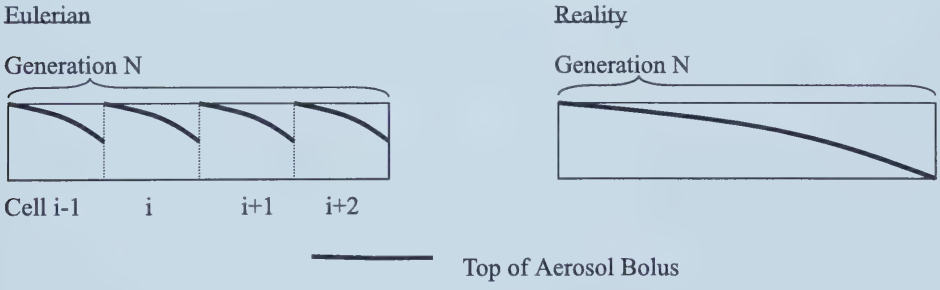

Figure 4.6: Remixing assumption necessary for Eulerian implementation

The dependency of the penetration fraction on the particle size can also be explained as a result of the remixing assumption. Settling occurs at the terminal velocity of each particle which increases in proportion to the size of the particle (see section 2.2.2.2). As a result, larger particles will be nearer the bottom of the tube when they are remixed. As the particle size increases, the apparent distance that a particle needs to travel to reach to bottom of the tube will correspondingly increase, thus reducing the expected deposition. The effect of the

homogeneous redistribution becomes increasingly significant as the particle size increases.

The significance of this approximation was examined by determining typical sedimentation parameters for the deposition tests to be done for this paper. Sedimentation is only calculated theoretically below the trachea, so T was determined in the model lung for each generation below the trachea for various flow rates. T is largest in the first generation after the trachea and decreases monotonically to the alveolar region. The value for T increases as the flow rate decreases and approaches 0.1 at a flow rate of 0.2L/min in this generation. Even for the smallest breath to be used, the flow rate is below 0.2L/min for less than 1% of the time. Consequently, the sedimentation parameter is below 0.1 throughout the entire domain for virtually all time. As seen in Figure 4.4, the difference in penetration fraction due to particle size below T=0.1 is less than 1%. Thus, the remixing assumption is deemed acceptable since T resides only in this region below 0.1 in all of the tests to be performed. However, this approximation is only valid for the continuous breathing without inter-breath pauses that are used in this study.

4.6.2 Comparison to RegDep and Published *in vivo* Data

TechAero was validated against the Lagrangian model, RegDep, using test conditions that can be accommodated by both programs. If the TechAero results compare favorably to the results obtained using RegDep, we can be confident in the use of TechAero for further tests containing variable boundary conditions that are impossible to simulate using the Lagrangian model. RegDep had also been previously validated against published *in vivo* data, thus TechAero can be further validated against this common background. The *in vivo* data, which is gathered in Stapleton, was obtained using gamma scintigraphic techniques and radiolabeled monodisperse aerosols [1,37,44–47].

TechAero was run using the same inputs as defined for the RegDep runs. Particle sizes of 0.25, 1.25, 2.25, 3.25, 4.25, 5.25, 6.25, 7.25, and 8.25μm were inhaled using a breath defined as follows: tidal volume = 700cc, inspiratory flow rate = 400cc/s, period = 4.0s, and duty cycle = 43.75%. Figures 4.7 through 4.9 display the *in vivo* data with the RegDep results overlayed with the TechAero results.

It is clear from Figure 4.7 that the TechAero results match both the *in vivo* data and the

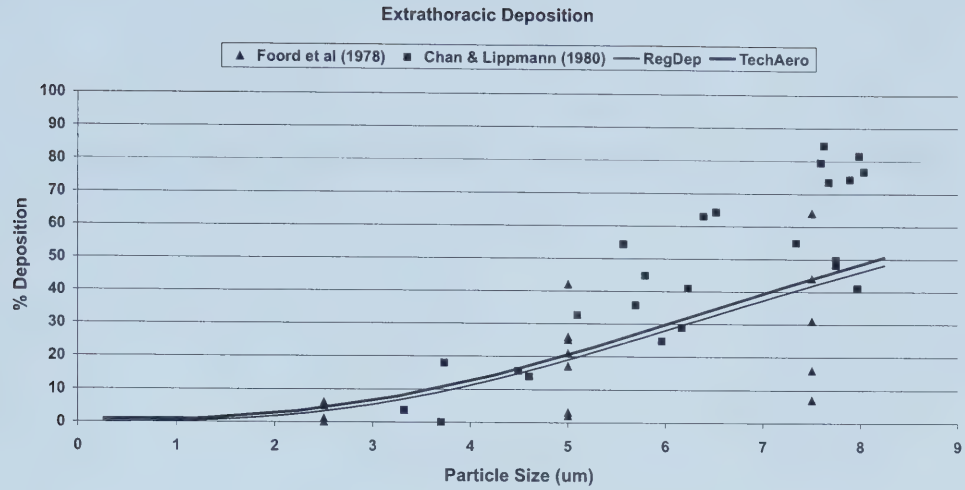

Figure 4.7: Extrathoracic deposition probability for TechAero, RegDep, and *in vivo* data

RegDep results quite well in the extrathoracic (ET) region. However, as seen in Figures 4.8 and 4.9 the TechAero results differ from the tracheo-bronchial (TB) and especially the alveolar (AL) deposition predictions of RegDep. Because of the improved match with the *in vivo* data in both these regions, we suggest this difference is an improvement over the RegDep Lagrangian calculations due to the inclusion of additional axial diffusion effects. Since the breath used in the original tests was quite shallow (700cc compared to the total lung volume ~3000cc) the aerosol could not penetrate much farther than the depth of the breath in a Lagrangian model such as RegDep. By being able to incorporate an effective axial diffusion, caused by Taylor diffusion [48] and secondary flows, TechAero's Eulerian model is able to better represent the deeper penetration and deposition actually experienced by the particles. Thus, compared to RegDep, TechAero would be expected to compute increasingly larger deposition percentages in the lower reaches of the lung for common breath volumes.

This explanation is evidenced by the increased separation between the TB and AL simulation results and further supported by running RegDep with a similar breath having a larger tidal volume of 2000cc. The third data line in Figures 4.8 and 4.9 (labelled: RegDep (Large Breath)) displays how this increased tidal volume allows the aerosol in the RegDep calculations to penetrate deeper and raise the deposition in the TB and AL regions to compensate for the lack of axial diffusion.

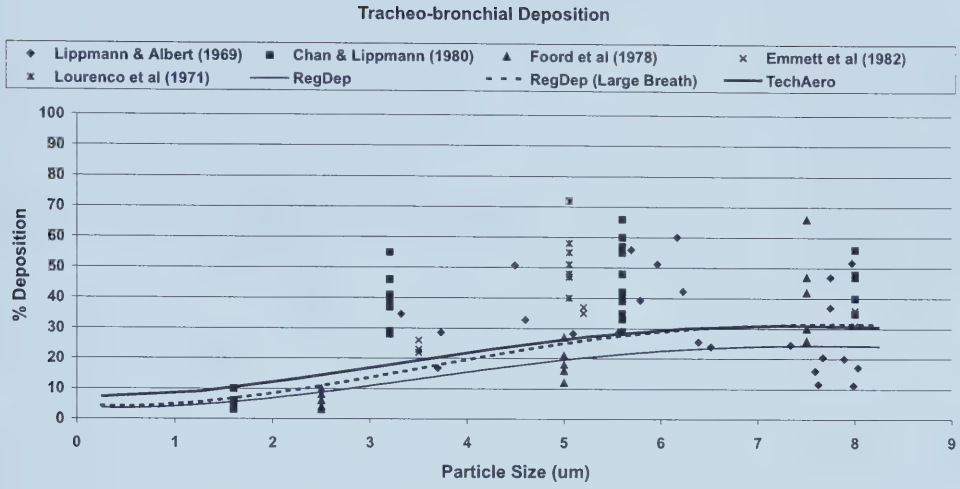

Figure 4.8: Tracheo-bronchial deposition probability for TechAero, RegDep, and *in vivo* data

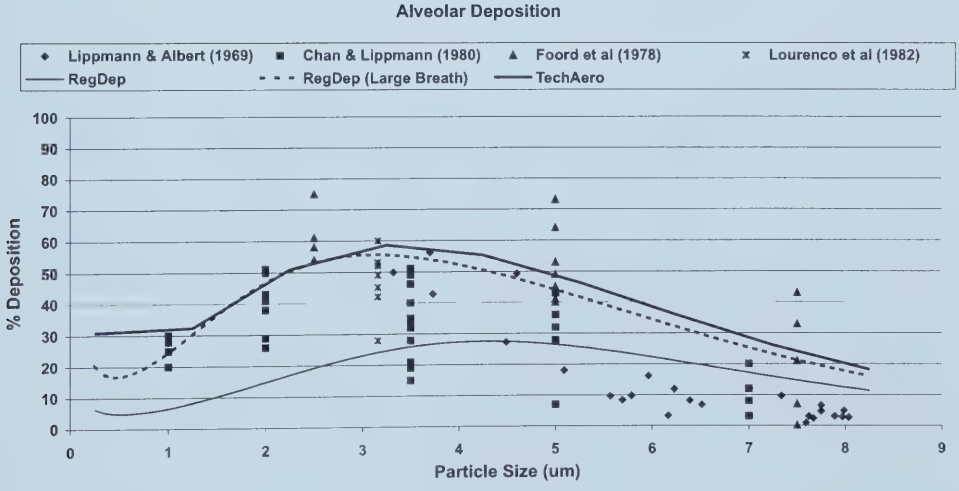

Figure 4.9: Alveolar deposition probability for TechAero, RegDep, and *in vivo* data

Chapter 5

Results and Analysis

5.1 Introduction

This chapter presents the results and analysis of each of the three stages of this research. This first section describes the processing of the collected breathing patterns, the comparison of the differences resulting from different types of breathing and finally the selection of breathing patterns to be used in the second stage. The second section presents the results of the standardized bench testing. The variables of interest for the bench tests are the amount of saline collected on the filter, the amount of saline left in the nebulizer, and the particle size distribution of the aerosol leaving the device. The third section examines the results of the Eulerian numerical simulation. The primary output of interest from the simulation is the regional deposition of the drug in the lung.

5.2 Part I – Examination of Breathing Patterns

The first step in the analysis involved interpreting and processing the plethysmograph output. A Fortran program (see Appendix C for a description of the algorithm used) was written to perform the conversion and averaging of the raw data into single representative waveforms, more useful for study and analysis[1]. Difficulties that arose and decisions that were made regarding the development of the algorithm will be described in the following sections.

[1]The program was originally written by Cam Shute but was unfinished and had to be extensively modified for use in this study.

5.2.1 Processing a Representative Average Breath

The averaging of the full breathing signal was not a simple task. What is the average of a series of waveforms? Is seems like a simple question if only the average tidal volume and period are of interest. In this study, however, the waveshape itself is of great importance and performing simple arithmetic averaging completely wipes out any waveshape information. Figure 5.1 shows an example wave and its mirror image summed and averaged at each point. The resultant average waveform is plainly unacceptable as it bears no resemblance to either of the initial curves.

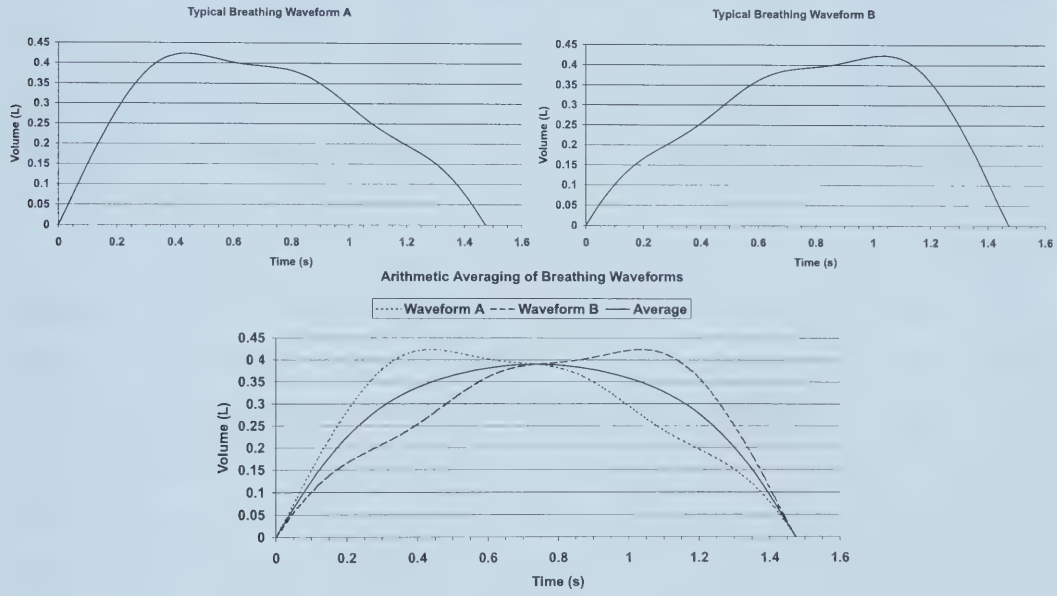

Figure 5.1: Unrealistic nature of arithmetic averaging for breathing patterns

While it is easy to obtain average values for standard breathing parameters, such as tidal volume (V_T) and period (T_T), it is clear that an average functional shape can only be obtained from waveforms that are similar in shape to begin with. Anything else results in a meaningless waveform. Some method other than arithmetic averaging must be implemented in order to obtain a meaningful representative waveform.

As a result, waveform averaging was accomplished in two ways. First, arithmetic averaging was done to obtain average values for the primary waveform-independent breathing parameters (V_T and T_T) using the full breathing data sample for each subject. Second, a

segment of steady breathing with consistent waveshape was used to obtain the functional waveform for the average breath. In this way, the standard waveform-independent breath parameters from the full data set can be used to compare with previously published results and to verify the validity of the average waveforms obtained from the segment data.

5.2.1.1 Manipulation of the Raw Waveforms

Several characteristics of the raw trace made forming a representative average difficult. Aside from the expected inter-breath variation in V_T and T_T, the waveforms generally exhibited slow drifts in the residual lung volume baseline. More concerning, however, was the presence of significant irregularities in many of the breathing traces. Most subjects had one or several sighs in their breathing signal which were significantly larger than other breaths. Additionally, other major irregularities, where the trace was completely different from the majority of the remaining breaths, were found.

The averaging program had great difficulty in dealing with these abnormalities. The irregularities may be artifacts from a subject swallowing or laughing for example and inclusion of these artifacts contributes nothing to the development of a standard "average breath". As a result, the sighs (defined as a breath volume greater than 2 times the average tidal volume) and other irregularities were manually removed from the raw data trace. This manipulation of the raw data is not unprecedented and has been carried out by other researchers examining human breathing pattern characteristics [14, 20].

5.2.2 Comparison of Normal and Nebulizer Breathing

5.2.2.1 Full Data Set

Effect on standard breathing parameters – The raw data was separated into individual breaths and the average tidal volume (V_T) and period (T_T) were determined arithmetically. The average period was determined by simply summing the lengths of each individual breath and dividing by the number of breaths considered. The average tidal volume is slightly more challenging in that the maximum volume is not reached at the same point in each breath. As a result, the point of maximum volume is determined for each breath, and again, summed and divided by the total number of breaths. Additional parameters such as the breathing frequency (f) and minute ventilation (V_{min}) can be determined from V_T and

T_T. A full table of the average values for each subject can be found in Appendix B while the averages for all the subjects are compiled and summarized in Table 5.1.

Normal Breathing	Tidal Volume (L)	Total Time (s)	Frequency (breaths/min)	Minute Ventilation (L/min)
Average	0.613	3.24	18.74	11.38
Std Dev	0.119	0.38	2.24	2.05
Nebulizer Breathing	Tidal Volume (L)	Total Time (s)	Frequency (breaths/min)	Minute Ventilation (L/min)
Average	0.791	4.38	14.31	10.75
Std Dev	0.279	0.94	3.23	2.81

Table 5.1: Summary of average breath parameters for normal and nebulizer breathing

A matched pair analysis was performed on the data in Table 5.1 to quantify the differences between the normal and nebulizer breathing. Again, matched pair data for each subject can be found in Appendix B while Table 5.2 summarizes the difference in means between normal and nebulizer breathing for the entire sample group for the confidence interval $P<0.05$.

Difference: Neb-Norm	Tidal Volume (L)	Total Time (s)	Frequency (breaths/min)	Minute Ventilation (L/min)
Average	0.178	1.139	-4.43	-0.64
Std Dev	0.243	0.942	3.51	2.67

Table 5.2: Matched pair, difference in means analysis for full breath data

The effect of breathing through a nebulizer had the following changes: V_T was increased by 178mL or 29% and T_T was lengthened by 1.139s or 35% with an accompanying decrease in breathing frequency. The change in V_{min} did not follow any particular trend with some increasing, some decreasing and one remaining virtually unchanged. These observed tendencies confirm previously published results regarding the effect of apparatus on breathing [20–27].

5.2.2.2 Segment Data Set

The same algorithm as in section 5.2.2.1 was used to determine the average waveform. To obtain an average functional shape, however, the raw breathing waveforms were manually examined for a suitable segment of consistently similar breaths. For each subject a section

of between 6 to 18 breaths was used to create the representative waveform. Below are two samples to demonstrate the effectiveness of this averaging. They each show the raw volume trace and the resultant average waveform replicated over several periods. Note that the first and last breaths from the raw segment are not included in the average. Figure 5.2 shows a segment from the *mikem* (see section 5.2.3 for an explanation of the waveform labelling) normal breathing signal with the elimination of the baseline drift clearly visible. Figure 5.3 shows a segment from the *brads* normal breathing trace with the small variations in V_T and T_T removed. Most importantly, the integrity of the original waveshape is maintained.

Effect on standard breathing parameters – Again, changes to the standard breathing parameters were examined. Similar to the previous section, only the group averages are presented in Table 5.3. Once again, a matched pair analysis was performed ($P<0.05$) with the average difference between normal and nebulizer breathing summarized in Table 5.4. Specific data for each subject can be found in Appendix B.

Normal Breathing	Tidal Volume (L)	Total Time (s)	Frequency (breaths/min)	Minute Ventilation (L/min)
Average	0.567	3.003	20.21	11.48
Std Dev	0.102	0.324	2.31	2.62
Nebulizer Breathing	Tidal Volume (L)	Total Time (s)	Frequency (breaths/min)	Minute Ventilation (L/min)
Average	0.760	4.184	14.96	10.81
Std Dev	0.273	0.898	3.21	2.71

Table 5.3: Summary of average breath parameters for a segment of normal and nebulizer breathing

Difference: Neb-Norm	Tidal Volume (L)	Total Time (s)	Frequency (breaths/min)	Minute Ventilation (L/min)
Average	0.193	1.180	-5.24	-0.67
Std Dev	0.249	0.921	3.64	3.25

Table 5.4: Matched pair, difference in means analysis for segmented breath data

The same trends are observed with slightly different magnitudes. In this case, V_T increased by 193mL or 34% and T_T was lengthened by 1.180s or 39%. Again, a trend in the change in V_{min} could not be established. The similarity of these trends to those from the

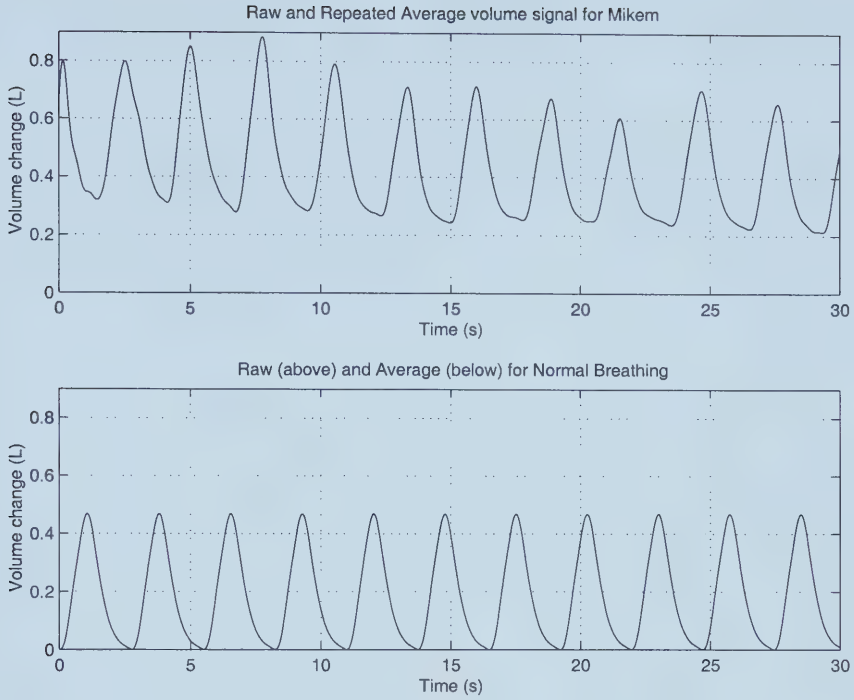

Figure 5.2: Comparison of repeated average waveform and original raw volume for *mikem*

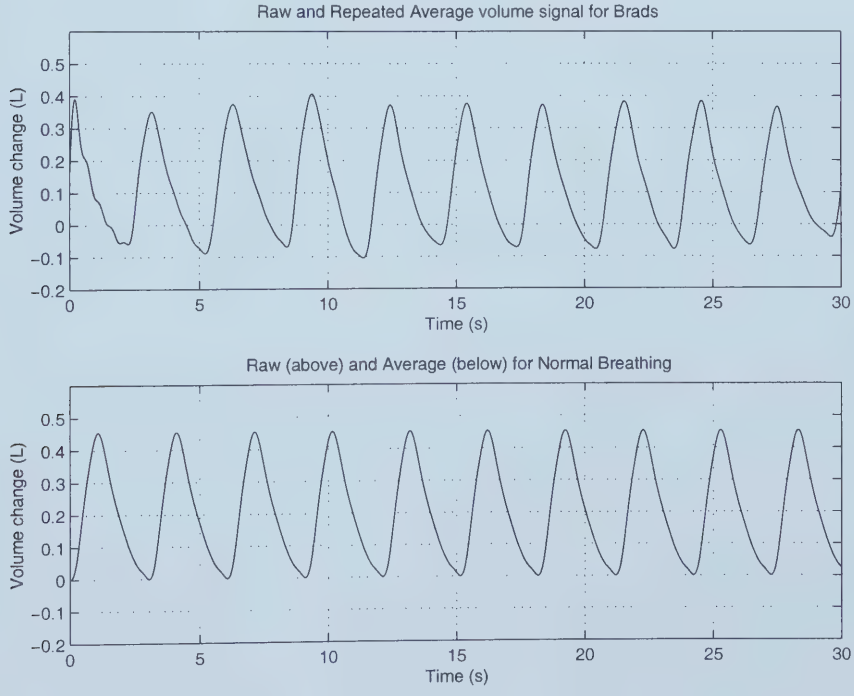

Figure 5.3: Comparison of repeated average waveform and original raw volume for *brads*

full data set aid in establishing the validity of the waveforms obtained from the segment data set.

Effect on functional shape – With the validity of the waveforms affirmed for these segment averages, we can further the comparison by looking at more shape dependent parameters. A qualitative comparison of the waveforms under study led to the specific examination of the inhale and exhale times and the corresponding duty cycle in addition to the mean inspiratory flow and the point of maximum flow. The group averages are found in Table 5.5 and the matched pair analysis ($P<0.05$) results are found in Table 5.6.

Normal Breathing	Inhale Time (s)	Exhale Time (s)	Duty Cycle	Inhale Flow Peak	Exhale Flow Peak	Mean Insp. Flow (L/min)
Average	1.276	1.727	0.425	0.483	0.223	27.24
Std Dev	0.187	0.244	0.048	0.111	0.045	6.48
Nebulizer Breathing	Inhale Time (s)	Exhale Time (s)	Duty Cycle	Inhale Flow Peak	Exhale Flow Peak	Mean Insp. Flow (L/min)
Average	1.982	2.202	0.478	0.347	0.330	22.56
Std Dev	0.389	0.631	0.055	0.083	0.074	4.74

Table 5.5: Group averages for waveshape dependent parameters

Difference: Neb-Norm	Inhale Time (s)	Exhale Time (s)	Duty Cycle	Inhale Flow Peak	Exhale Flow Peak	Mean Insp. Flow (L/min)
Average	0.706	0.475	0.053	-0.136	0.107	-4.64
Std Dev	0.390	0.654	0.061	0.128	0.095	6.06

Table 5.6: Matched pair, difference in means analysis on wave dependent parameters for segmented breath data

The examination of these timing parameters presented some interesting and unexpected results. An increase in inhale time, with a change of 0.706s or 55%, is seen to contribute more to the overall increase in breath period than the increase in exhale duration, with a change of only 0.475s or 28%. This unequal variation in each breath phase further leads to a shift in the overall duty cycle. Normal breathing is characterized by unequal phase durations with a duty cycle ratio typically around 0.4. In this test, the normal breathing patterns exhibited an average duty cycle of 0.425 while breathing through a nebulizer caused the duty cycle to shift towards a more balanced breath, exhibiting a duty cycle of 0.478. This marks a change of 0.053 or 12%. Additionally, the period increased at a greater rate

than the tidal volume resulting in an overall change in the average inspiratory flow rate of -4.64L/min or -17%.

Finally, a nearly overlooked trend was in the relative position of the flow peak in a breath. The position of the flow peak is defined as the fraction of time for the flow to increase to its maximum relative to the total time of either the inhale or exhale. The switch to nebulizer breathing was observed to shift the flow peaks towards the beginning and end of the breath for the inhale and exhale respectively. In other words, the separation between the flow peaks widens with nebulizer breathing. This shift was quantified and confirmed to be statistically significant by the matched pair analysis. The shift in the inhale peak was -0.136 or -28% while the exhale peak shift was 0.107 or 48%. This can be more clearly understood by referring to a typical flow rate curve. Figure 5.4 shows the inhale and exhale flow curves for the *brads* breathing patterns. The normal and nebulizer patterns are normalized in time and volume to isolate the shape effects and to display this peak shift graphically.

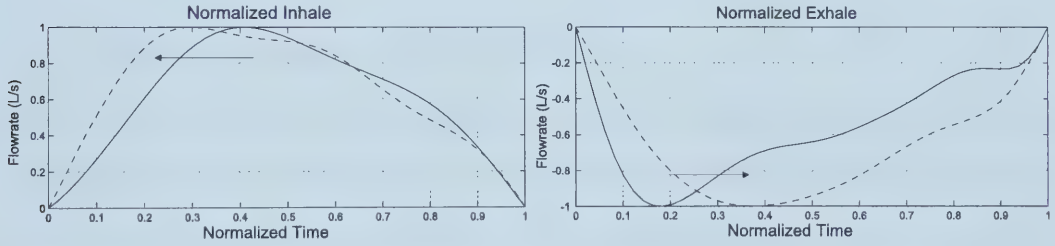

Figure 5.4: Flow peak position for normal (——) and nebulizer (- - - -) breathing

5.2.3 Selection of breathing patterns

Three subjects breathing patterns were selected from the original twelve to participate in the bench testing. The normal and nebulizer patterns for the three chosen subjects were the most significantly different from each other or from sine or square waves. If no significant effects are found due to these most significantly different waveforms then testing the less different waveforms would be redundant.

As mentioned in section 3.2.3, the testing was done using four-breath sets. Each subject had two four breath sets consisting of a sine wave, a square wave and the subjects normal and nebulizer breathing patterns. One set was normalized to a common period, tidal volume,

and duty cycle corresponding to the average parameters for the subjects normal breathing pattern while the second set was normalized according to the average nebulizer parameters. This normalization method guarantees a constant minute ventilation and average inspiratory flow rate within each test set and specifically isolates the shape effects we wish to examine. A Matlab program (*scalerflow.m*) was written to perform the normalization and the algorithm can be found in Appendix C.

The waveforms are named according to the subjects first name and last initial with a suffix defining the normalization parameters used (eg. *bradsneb* - denotes the 4 breath set comprised of a sine wave, a square wave and *brads* normal and nebulizer waveshapes normalized to the average values for *brads* nebulizer breathing parameters, whereas *bradsnorm* denotes the set normalized to *brads* normal breathing parameters). The six tested breath sets from the three subjects are displayed on the following pages in Figures 5.5 through 5.10. The differences in waveshape are made apparent when plotted on these normalized scales.

5.3 Part II – Bench Test Results

Three resultant outputs were considered from the bench tests. 1) The amount of saline collected on the filter, 2) The amount of saline left in the nebulizer, and 3) the particle size distribution of the aerosol leaving the device. The results concerning saline amounts will be considered first.

Note also, that we assume any saline not making it to the filter and not remaining in the nebulizer is exhaled through the outlet valve on the mouthpiece. Preliminary tests involving the assay of the internal surfaces of the connection tubing and the PDA window produced negligible amounts of saline and confirm the validity of the above assumption. As such, only the saline on the filter and left in the nebulizer will be considered.

5.3.1 Saline Amounts

5.3.1.1 Error Correction

The measured saline amounts collected on the filter are expressed as a percentage of the initial charged dose in the nebulizer. The measured saline amounts, however, need to be corrected in two ways. The measured mass on the filter is adjusted according to the ex-

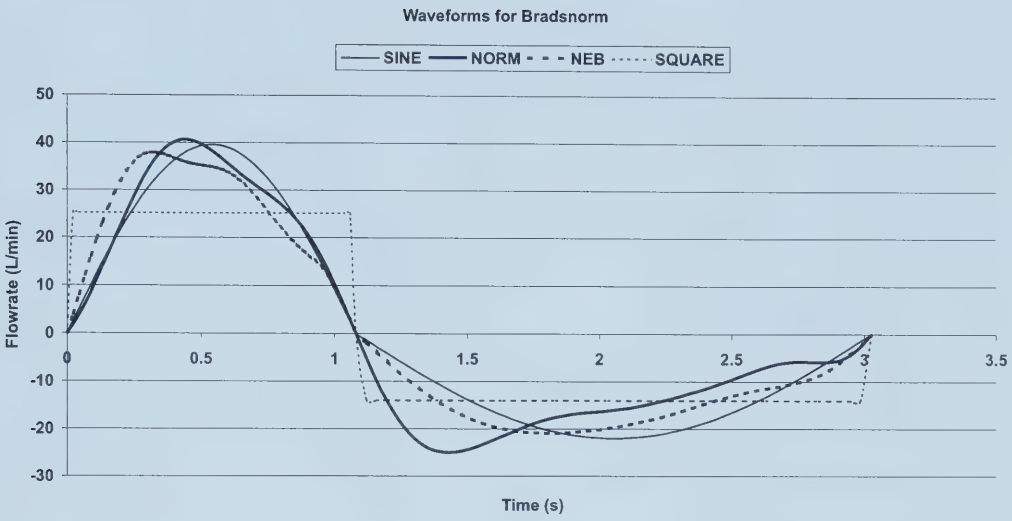

Figure 5.5: Breathing pattern set for *brads* normalized to "normal" breath parameters

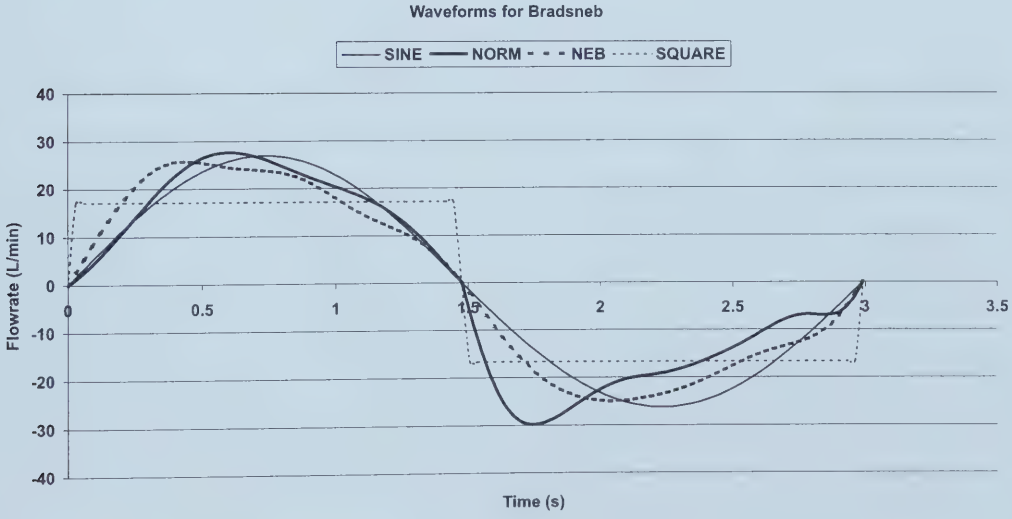

Figure 5.6: normalized to "nebulizer" parameters

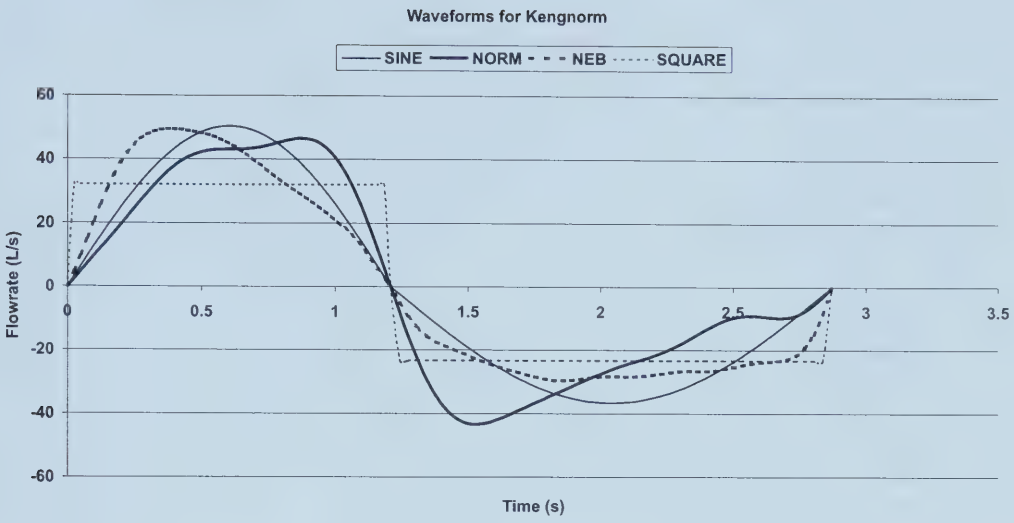

Figure 5.7: Breathing pattern set for *keng* normalized to "normal" breath parameters

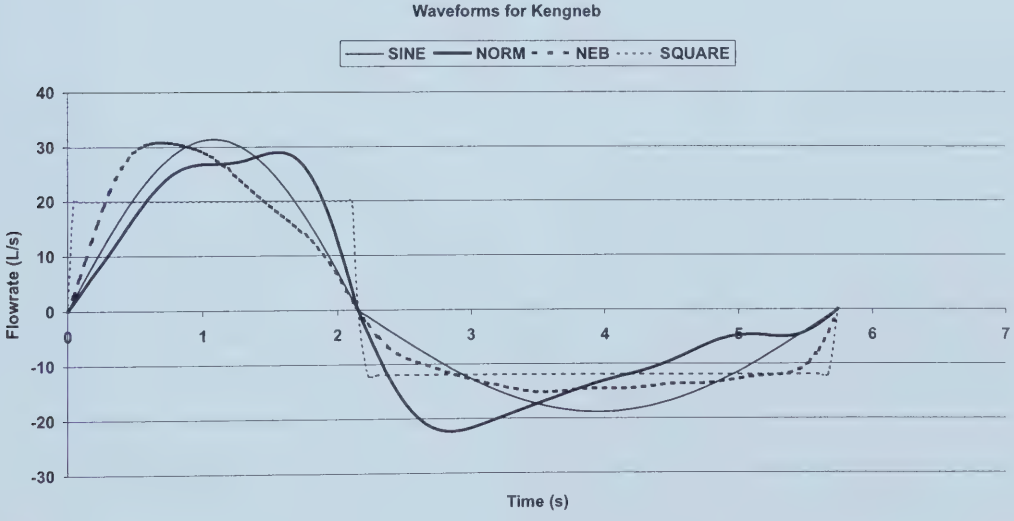

Figure 5.8: normalized to "nebulizer" parameters

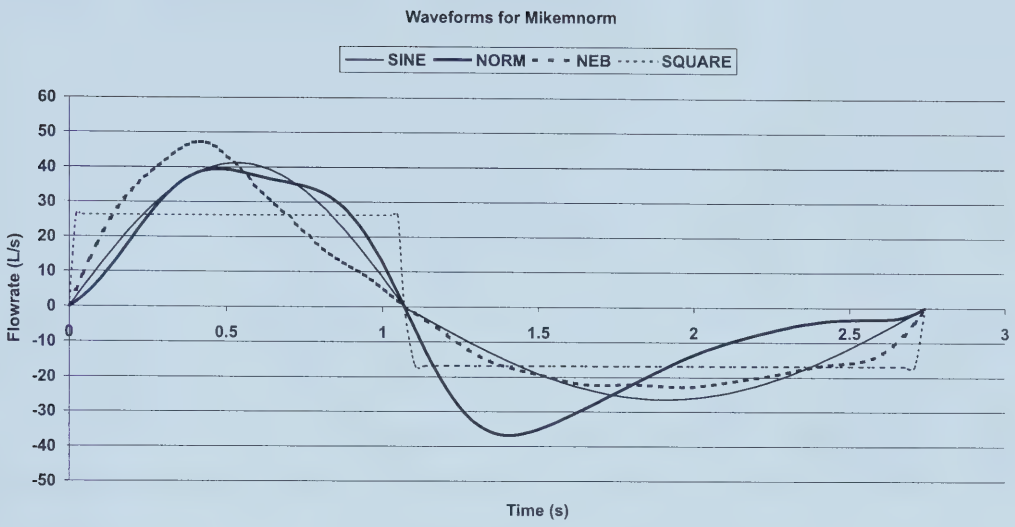

Figure 5.9: Breathing pattern set for *mikem* normalized to "normal" breath parameters

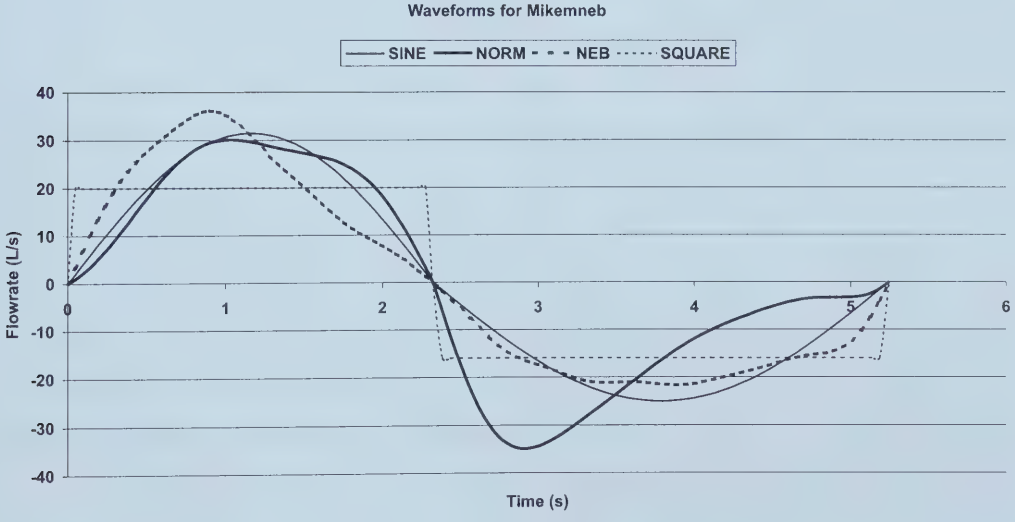

Figure 5.10: normalized to "nebulizer" parameters

traction error determined in section 4.5 on page 36 and further adjusted by the connection volume correction shown in Equation 5.1 below [28].

$$m_{corrected} = \frac{V_T}{V_T + V_{dead}} m_{measured} \tag{5.1}$$

where $m_{corrected}$ — mass on filter corrected for connection volume effects [mg];
$m_{measured}$ — measured mass on filter [mg];
V_T — tidal volume of breathing pattern [mL];
V_{dead} — connection volume [mL];

The connection volume for this bench setup was 60mL and consisted of the connection tubing, the PDA measurement window, and half of the filter housing (see Figure 3.2 on page 20). The resultant connection volume correction ranged from a 16% increase for the smallest breathing pattern to 8% for the largest while the extraction error correction ranged from 12.6% to 2.6%.

5.3.1.2 Filter Results

The corrected mass trapped on the filters for each test set are summarized in Figure 5.11 on page 58. The graph is plotted according to each four breath set with the error bars indicating the standard error from the tests. The fifth data series is plotted according to the secondary axis and shows the minute ventilation to aid in the discussion to follow. An analysis of variance (ANOVA) was done to compare the test results statistically ($P<0.05$). Only the waveforms for *kengneb* and *kengnorm* resulted in statistically significant differences in the nebulizer output.

5.3.1.3 Residual Nebulizer Results

The amount of saline left in the nebulizer is not affected by the connection volume error. Any extraction error present is disregarded as negligible as it should have no consequence on the conclusions drawn since the amounts are nearly the same for each case. The residual saline left in the nebulizer for each test set is shown in Figure 5.12 on page 58. Again, ANOVA analysis was done, this time finding no statistical differences ($P<0.01$) in the residual amount of saline left in the nebulizer within each test set.

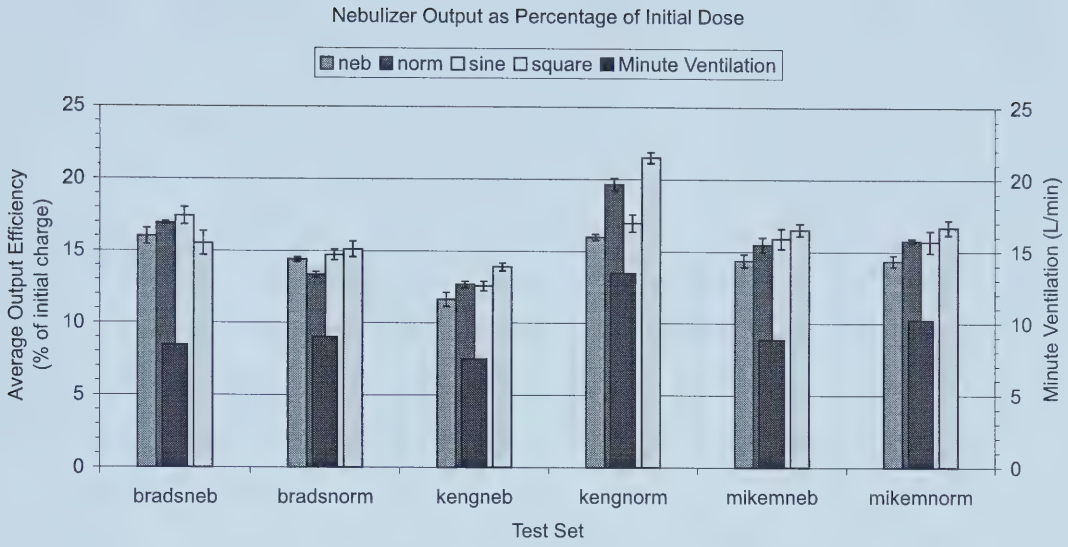

Figure 5.11: The amount of saline collected on the filter

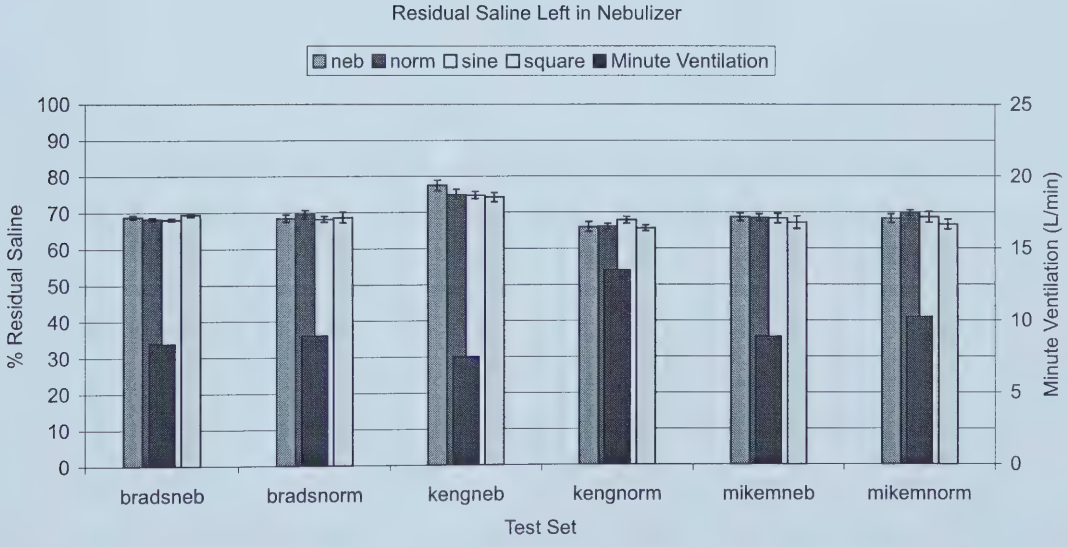

Figure 5.12: The amount of saline remaining in the nebulizer at the completion of each test

5.3.1.4 Analysis and Discussion

Because the Pari LC⋆ is a breath enhanced nebulizer, differences in minute ventilation alone would likely have a large effect. This is exactly why each breathing pattern within a set was normalized to a common minute ventilation. This base level dependence on the total amount of air inhaled during the test is evidenced by the residual amounts left in the nebulizers (Figure 5.12). The breathing pattern set with the largest minute ventilation (*kengnorm* – 13.5L/min) resulted in the least amount of saline left in the nebulizer (66%) while the one with the smallest minute ventilation (*kengneb* – 7.5L/min) had the most saline remaining (75%). The other breathing patterns each having a minute ventilation between these two extremes all had similar residual amounts (between 68-69%) that were not statistically different (P>0.01).

Similarly, the amount of saline reaching the filter should also scale according to V_{min}. As expected, the tests resulting in the most and least saline on the filter correspond to the breathing patterns with the largest and smallest V_{min} respectively (*kengnorm* and *kengneb*). However, the remaining breathing patterns do not follow this trend. The minute ventilation for the two breath sets for *brads* are 8.46L/min for the nebulizer normalized patterns and 9.00L/min for the normal normalized patterns. These are similar in magnitude and we would expect similar amounts of saline reaching the collection filter. As seen in Figure 5.11, however, this is not the case. The set with the smaller V_{min} actually has a higher average output efficiency, 16.5% compared to 14.3%. Alternatively, the two *mikem* breath sets have quite different minute ventilations of 8.87 and 10.24L/min yet, within roundoff, have identical output efficiencies of 15.6%. A factor other than minute ventilation must be contributing to the nebulizer output efficiency differences.

It is proposed that the difference in breath duty cycle is responsible for these differences. The two *brads* breath sets have quite similar V_T and T_T resulting in similar minute ventilation. Thus the only variation between the two complementary sets is in the duty cycle. The set with the longer (0.493 compared to 0.357) duty cycle caused an increase in nebulizer output efficiency opposite to what would be expected considering only minute ventilation. This effect would also explain the identical output efficiencies resulting from the complementary *mikem* sets with different minute ventilations. In this case, the set with

the smaller minute ventilation had the longer duty cycle (0.443 compared to 0.390). These opposing factors resulted in identical output efficiencies for this pair of sets.

Among each pair in both of the above cases, the wave set with the shorter duty cycle was less efficient in getting saline to the filter than would be expected based solely on V_{min} considerations (see Table 5.7). It appears that a longer duty cycle has the effect of increasing nebulizer output. During exhalation, the mouthpiece valve is opened while aerosol is continually being produced and lost to the environment (see section 2.3.2 on page 14). Simply put, the shorter the duty cycle, the longer the exhale valve is opened and the more saline is exhausted to the environment. This inference is further supported by the constancy of the nebulizer saline residual within a test set. The difference in saline not making it to the filter is not being left in the nebulizer, but rather, is being exhaled through the mouthpiece valve.

	V_{min} (L/min)	Duty Cycle	Average Output Efficiency (%)
bradsneb	8.46	0.493	16.5
bradsnorm	9.00	0.357	14.3
mikemneb	8.87	0.443	15.6
mikemnorm	10.24	0.390	15.6

Table 5.7: The effect of duty cycle on average nebulizer output efficiency

A qualitative examination of the waveforms and output efficiency revealed two trends. First, the square wave patterns resulted in the highest output efficiency in every case except one. Second, the output efficiency of the other more smoothly varying curves appears to correlate with the location of the flow peak during the inhale phase of the breath since the only variation within a breathing pattern set is the wave shape between the zero crossings of the flow. The later that maximum flow is reached during the inhale time, the greater the output efficiency. Table 5.8 summarizes this result by arranging the breathing patterns within each test set in order of increasing relative position of the flow peak within the inhale period. It is clear from examining the tested waveforms in Figures 5.6 to 5.9 beginning on page 54 that the output efficiency follows this trend in every pattern set except for one anomalous case. This effect could be due to a buildup of aerosol in the nebulizer before the maximum breathing flow is reached. As the flow peak occurs later in the inhale period the aerosol is able to build to a greater amount before being inhaled onto the filter.

Subject	Breathing pattern	Relative position flow peak $\frac{t_{peak}}{t_{inhale}}$	Average output efficiency (%)	
			nebulizer test set	normal test set
brads	neb	0.306	16.0	14.4
	norm	0.408	16.9	13.4
	sine	0.5	17.4	14.7
keng	neb	0.327	11.6	16.0
	sine	0.5	12.6	17.0
	norm	0.714	12.7	19.7
mikem	neb	0.388	14.4	14.4
	norm	0.449	15.5	15.8
	sine	0.5	15.9	15.7

Table 5.8: The effect of the position of maximum flow on average nebulizer output efficiency

The final points to consider comment on the significance that breathing pattern differences have on nebulizer output efficiency. It appears that these effects scale with V_{min}. Both of the *keng* test sets produced statistically significant output differences yet the *kengnorm* test set produced much more drastic differences presumably due to the larger V_{min}.

As stated above, the two breathing pattern sets that caused statistically significant differences were the *kengneb* and *kengnorm* test sets which, incidentally, were qualitatively considered to contain the most significantly different breathing waveforms. The other test sets which had less variation in the component breathing patterns resulted in statistically insignificant differences. It is unclear how different a breathing pattern must be from, say, a standard sine wave shape before it produces output efficiency variability.

Finally, the level of device dependent variability must be considered. Every breathing pattern test was repeated using four separate nebulizers. Closely examining the individual test results revealed that nebulizer #3 generated significantly lower output efficiencies in 14 of the 24 tests performed. It has to be realized that this sort of device inconsistency could swamp any variability due to breathing pattern differences.

5.3.1.5 Summary

Differences in nebulizer output efficiency due to differences in breathing pattern were observed throughout these tests. In addition to the expected scaling of output efficiency with the V_{min} of the breathing pattern used, the actual functional shape of the breath can affect the output efficiency as well. Variations in duty cycle had a large effect on the output effi-

ciency while the location of the flow peak in the inhale affected the amount of saline inhaled from the nebulizer but not the amount left behind after nebulization. Noticeable inter-device variability was also observed in repeating tests while changing only the nebulizer used.

5.3.2 Particle Size Distribution

The particle size data obtained from the Dantec PDA system can be analyzed in several ways. First, how the size distribution varies due to the four nebulizers used in testing each breathing pattern, second, how it changes over the course of the five minute test, third, how it varies across a test set, fourth, how it varies between test sets, and fifth, how the particle size distribution changes over the course of a single breath.

A common assumption in aerosol testing is that the particle size follows a lognormal distribution. If this is the case than the output size of the tests can be represented by two simple parameters: the mass median diameter (MMD) and the geometric standard deviation (GSD). After confirming the validity of the lognormal assumption, the Matlab script *sizer.m* (see Appendix C for a summary of the algorithm used) was used to calculate the average MMD and GSD for each of the six 10 second samples obtained during every test.

5.3.2.1 Variation due to solution nebulization and device used

Comparing the results from each of the four nebulizers used gives a representation of the inter-device variability and the size changes over the course of nebulization. There was a small degree of inter-device variability but the results for the four nebulizers consistently remained within the Dantec accuracy from each other. Figure 5.13 shows the results from the sine waveform from the *mikemnorm* test set. Although the actual sizes may differ in magnitude among the test sets, this figure is indicative of the trends observed in all sets. Each line represents the particle size over the course of nebulization for each of the four nebulizers used. No consistent device dependence was observed.

Also notice from Figure 5.13 that the change in particle size over the course of the five minute nebulization does not follow any particular increasing or decreasing trend. Other studies have also shown that the output particle size neither increases nor decreases as nebulization progresses [49].

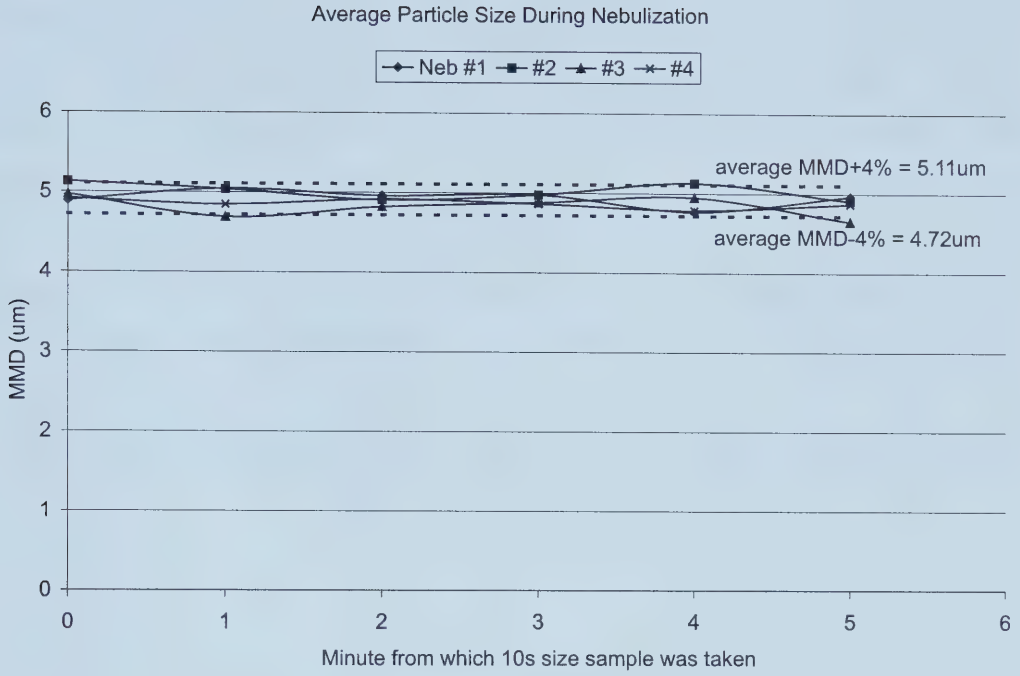

Figure 5.13: Particle size variation over the course of nebulization for each of the four tested nebulizers

5.3.2.2 Variation due to breathing pattern

The size differences within a test set are summarized in Table 5.9 and no apparent trends are observed. The Dantec PDA system has an accuracy of $\pm 4\%$ which for particles around 5μm equates to $\sim \pm 0.20\mu$m. It is clear that the average MMD for each breathing pattern within each test are within this 0.40μm range of one another in nearly every case. The few results outside of the accuracy range for a group were considered to be anomalous.

	Average Particle Size for Test Set (μm)					
Waveform	bradsneb	bradsnorm	kengneb	kengnorm	mikemneb	mikemnorm
neb	5.66	5.21	5.61	4.46	5.19	4.89
norm	5.51	4.81	5.94	4.73	5.14	4.92
sine	5.58	5.27	5.92	4.72	5.14	4.91
square	5.88	4.96	6.05	4.65	5.36	4.95
average	5.66	5.06	5.88	4.64	5.21	4.92

Table 5.9: The average particle size for each breathing waveform within each test set

There were, however, clear size differences between test sets. The nebulizer test set

waveforms are observed to produce larger particles than the subject's complementary normal test set. The average particle size appears to scale inversely with the average inspiratory flow rate of the breathing pattern. This is not unexpected due to baffle filtering processes described in section 2.3.1.3 on page 13. The largest particle size that is able to make it out of the nebulizer without impacting on the walls decreases as the flow rate increases. Table 5.10 displays this general trend with the test sets positioned in order of increasing flow rate. The average GSD for each test set, which can also been seen in Table 5.10, remained virtually constant with no statistically significant differences between any of the test runs (P>0.01).

Test Set	Mean Inspiratory Flow (L/min)	Average MMD (μm)	Average GSD
bradsneb	17.18	5.66	1.62
kengneb	19.99	6.05	1.62
mikemneb	20.02	5.36	1.60
bradsnorm	25.21	5.06	1.59
mikemnorm	26.30	4.95	1.62
kengnorm	32.09	4.65	1.57

Table 5.10: The average particle size and inspiratory flow rate for each test set

The slight inconsistency between the *bradsneb* and *kengneb* waveforms can be attributed to a difference in ambient test conditions. The ambient temperature and relative humidity has been shown to have an effect on the output particle size distribution of the nebulizers used in this study [15]. The *bradsneb* set was tested at a RH=30% while the *kengneb* tests were performed at RH=47%. These differences would cause the slightly inconsistent result between these waveforms as lower ambient relative humidity would increase hygroscopic shrinkage resulting in smaller output particle sizes than expected.

5.3.2.3 Variation over single breath

The Matlab script *sizer.m* was modified slightly to extract particle size changes over the course of single breaths. In addition to particle size, the PDA system also measures velocity based on the arrival and transit time of a particle across the measurement volume. A group of particles with negative velocity signal the beginning of the exhalation before the particles have had a chance to clear the measurement window. Thus, the particles measured between consecutive negative velocity groups constitute a single inhalation. The MMD was then calculated for every 500 consecutive particles within a single breath using the arrival time

data. Inter-breath size variation was determined over a single breath within every 10 second sample period.

The general trend is for the average particle size to be initially very large then quickly dropping to around the group average determined in the previous section. This can be explained by baffle size filtering described in section 2.3.1.3. As the breathing pattern begins, the flow is relatively slow and large particles can manage to make it out of the device. As the flow quickly ramps up, however, the largest possible particles successfully exiting the nebulizer will decrease. This is clearly seen in Figure 5.14, with the large initial tails quickly dropping down and fluctuating about the test average value.

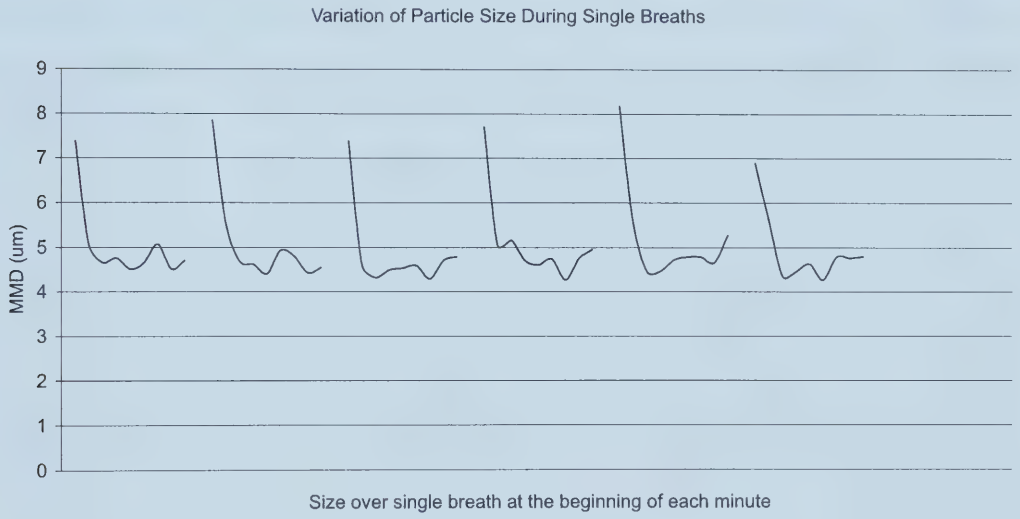

Figure 5.14: Typical particle size variation over the course of individual breaths for each 10s sample

If this is indeed the mechanism producing these results, then other characteristics of the size variations should be observed. First, the average size should tail up again at the end of the breath as the flow decreases to similar levels as the start of the breath. Second, the square wave tests should not show this initial size tail since the breathing pattern flows at a constant magnitude with no ramping up or down.

In fact, both of these characteristics do show up to some degree. In several cases, the beginnings of a rising tail are observed. This is reasonable due to the connection volume of the test set up that was used. As the flow ramps down at the end of an inhale the

resultant output particles begin to increase in size. As the exhale begins, however, these particles emitted near the end of the inhale are simply swept out of the exhale valve never having made it to the size measurement window. It is these same particles that also do not make it to the collection filter necessitating the connection volume correction implemented in section 5.3.1.1.

Figure 5.15 shows the lack of an initial size tail in the square wave tests. In the majority of cases a smaller or non-existent tail is observed. It is reasonable, however, to expect some degree of an initial size tail for a square wave breathing pattern as well. A true square wave cannot be reproduced exactly using the breathing machine due to limiting possible accelerations of the motor (see Figure 4.1 on page 34). Instead, there will also be a ramping up period and, if long enough, will produce a brief yet measurable increase in the output particle size.

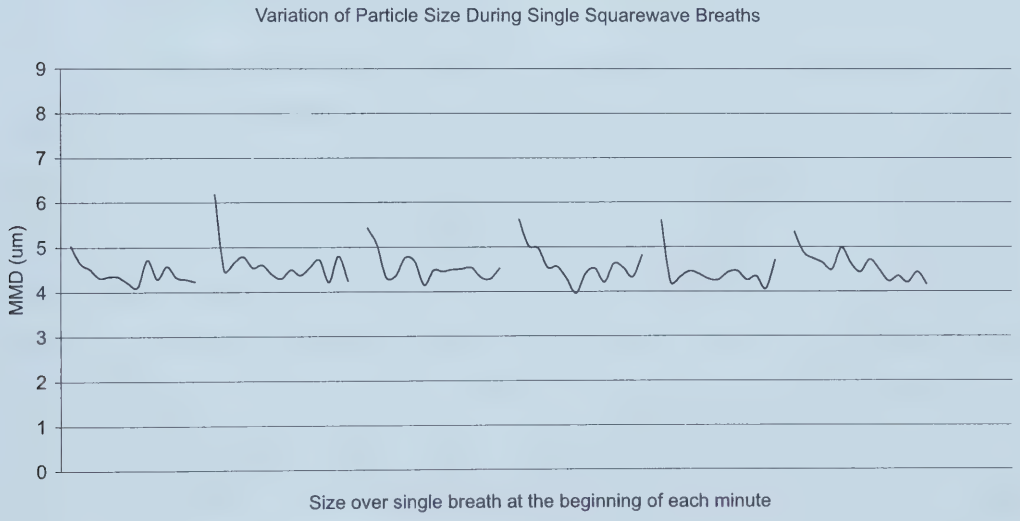

Figure 5.15: Typical particle size variation over the course of individual breaths for square wave breathing pattern

5.3.2.4 Summary

Differences in output particle size due to differences in breathing pattern were observed throughout these tests. However, the actual functional shape differences within test sets and the inter-device variability were not observed to have significant effects. Additionally,

the average particle size was not observed to have a consistent increasing or decreasing trend over the course of nebulization.

The output particle size is closely dependent on the flow rate through the device and size differences manifest themselves in two primary ways. First, recorded size differences arose between breathing patterns having differing V_{min} or more specifically, differing average inspiratory flow rates. The output particle size increased as the average inspiratory flow rate decreased. Second, it was observed that the size varies over the course of a single breath itself, being initially very large and then dropping down to the test-wide average value before appearing to rise again at the end of the breath. This tendency is reduced or eliminated when using square wave breathing pattern.

5.4 Part III – Computer Simulation Data

5.4.1 Regional Deposition Results

The deposition results for each lung region are presented in the following sections as percentages of the total aerosol inhaled. Preliminary testing revealed that varying the particle production rate affected the total inhaled amount and correspondingly the absolute amount of deposition in each region. The relative deposition percentages, however, remained unchanged. Since each test was run over the period of a single breath, scaling would be necessary to compare the absolute inhaled amount to that obtained by the *in vitro* bench testing. The particle production rate, however, needs to be calculated from the same total inhaled amount obtained through the bench testing of part two. Consequently, these circular calculations make comparisons of the absolute amounts meaningless and the average calculated production rate from all the tests of $5x10^4$ particles/s^{-1} was used as a common value throughout. The average MMD for each test set was used as input for each breathing pattern within the set. The average MMD's obtained from the bench testing can be found in Table 5.9 in section 5.3.2.2 on page 63.

The deposition in each region is presented as a percentage of the total inhaled amount for each breathing pattern within each test set in Figures 5.16 through 5.19.

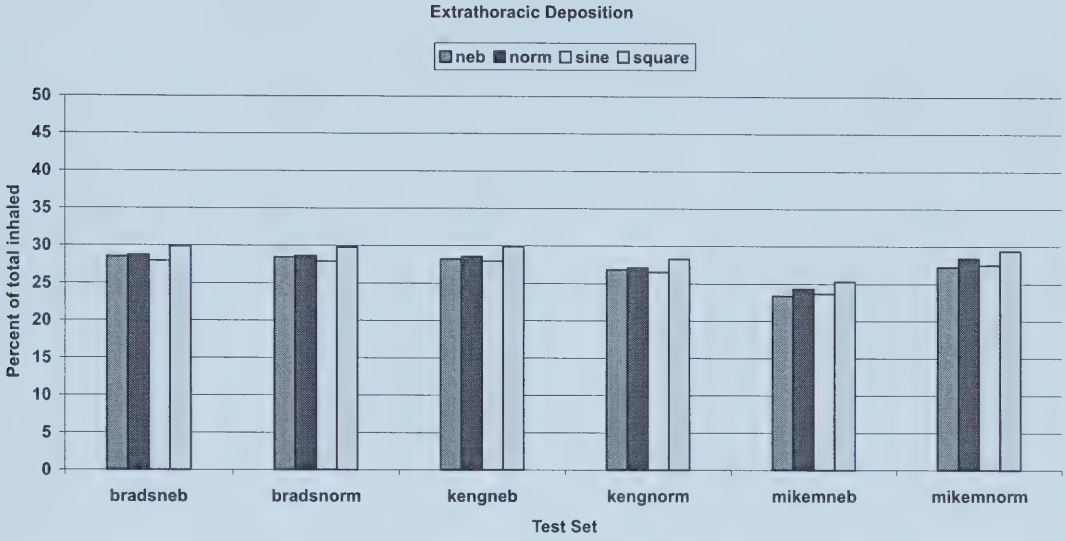

Figure 5.16: Extrathoracic deposition as a percentage of total inhaled amount

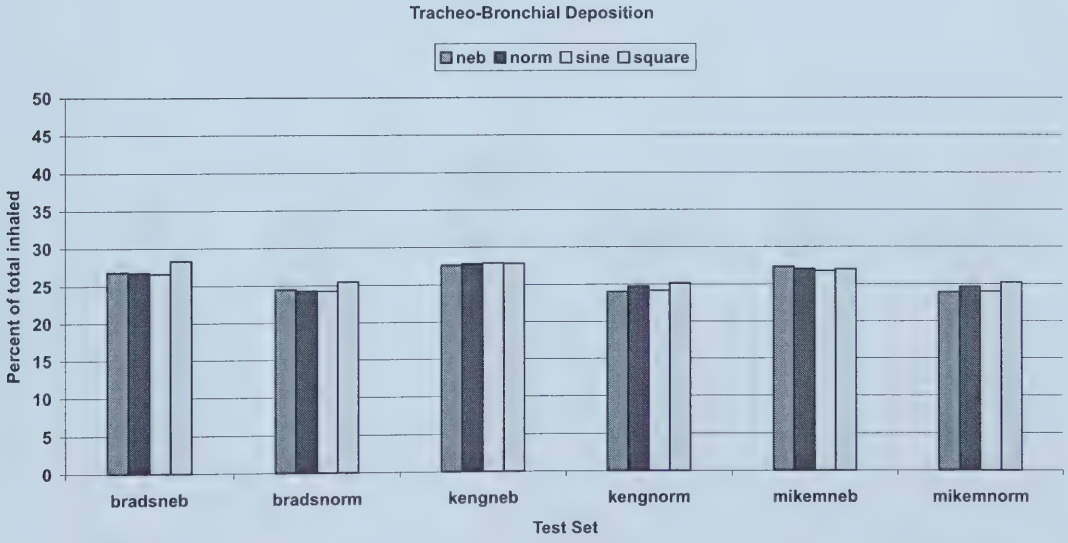

Figure 5.17: Tracheo-bronchial deposition as a percentage of total inhaled amount

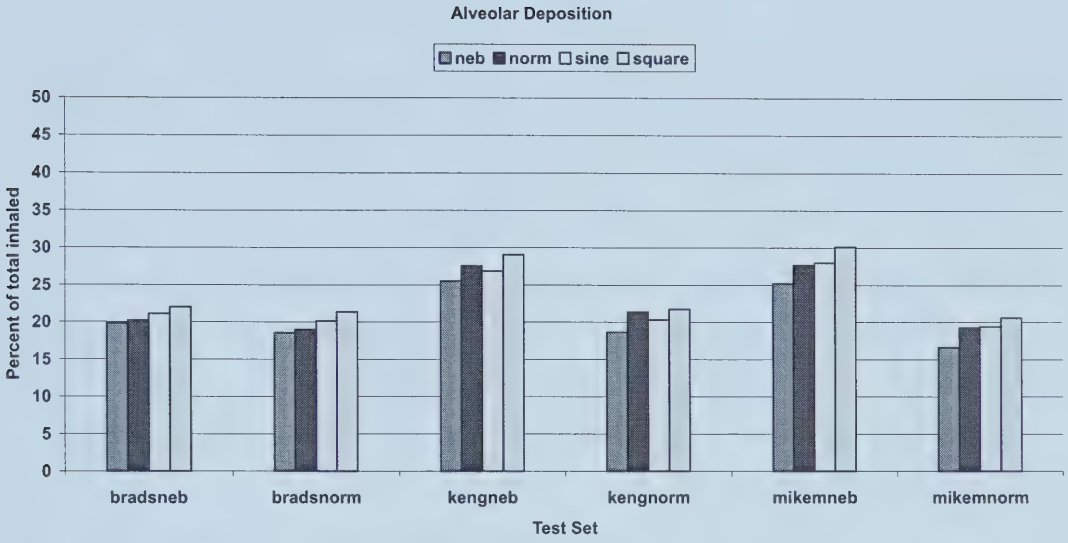

Figure 5.18: Alveolar deposition as a percentage of total inhaled amount

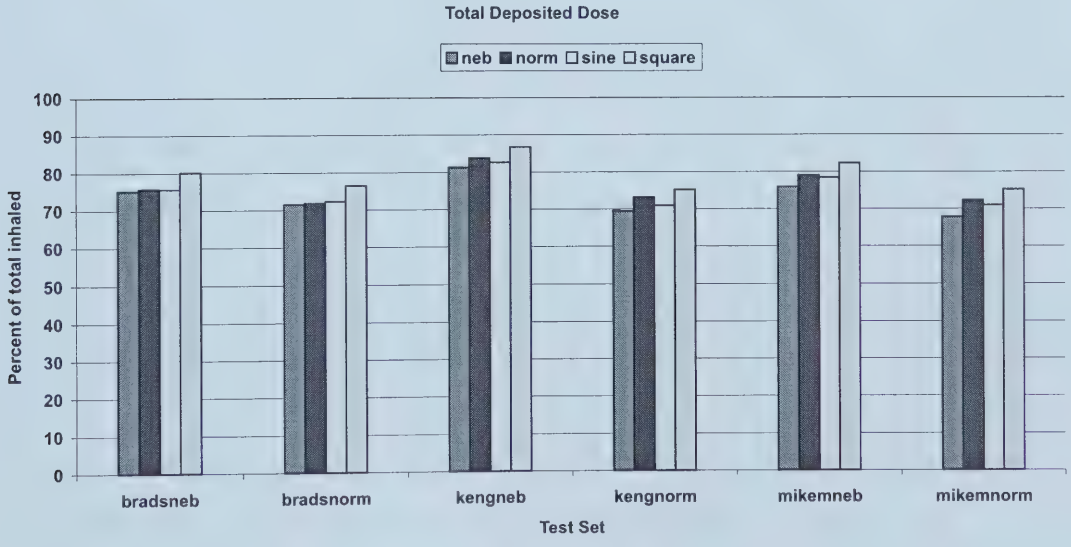

Figure 5.19: Total airway deposition as a percentage of total inhaled amount

5.4.2 Analysis and Discussion

5.4.2.1 Regional Lung Deposition

The actual functional shape of the breathing pattern does not appear to have any large significant effects on the regional deposition in the lung. Figures 5.16 to 5.19 did reveal, however, that the square waveform consistently resulted in higher deposition percentages in all regions for each test set, yet, the actual percent difference was small.

The deposition percentage in the extrathoracic region appears most insensitive to breathing variations with differences <2% for all breaths within each test set. The difference in the tracheo-bronchial region is <2% when considering all breaths within a set and <1% when ignoring the square waves. The alveolar region displayed differences <5% for all waves in a set and <3% without the square waves. Finally, the total lung deposition had differences approaching 7.5% with and 5% without considering the square waves.

5.4.2.2 Isolated Flow Effects

Each breathing pattern test was run using the average particle size obtained from the *in vitro* bench testing for each particular case. Thus, the differences observed above are the result of both the breathing pattern flow variations in the lung and the particle size differences resulting from flow variation through the nebulizer passed from part two of the study. While this setup is more accurate when considering the overall process of delivering drugs to the lungs from nebulizer to deposition, the effect of breathing variations independent of the particle size effects is of interest when considering testing using standardized particles. All of the above tests were repeated using a common initial MMD of 5μm.

The difference in deposition percentages between the test sets diminished slightly with the removal of the particle size variations. All percentages rose slightly if the original particle size was below 5μm or fell if the original size was above 5μm. The maximum deposition differences within test sets of 2%, 2%, 5%, and 7.5% remained unchanged for the extrathoracic, tracheo-bronchial, and alveolar regions and the total deposition respectively.

5.4.3 Combined Simulation and *in vitro* Bench Test Results

As was done for this research, nebulizers are commonly tested using both *in vitro* bench setups and computer simulations. The observed differences in each stage of the study were shown not to be statistically significant for the majority of the cases. The combined effect of these differences, however, may not be insignificant.

In the bench tests, compared to the results from the nebulizer breathing patterns, the square wave patterns overpredicted the total inhaled saline by 2.1% on average. Similarly, TechAero overpredicted the regional dosages by 1.64%, 0.79%, and 3.43% in the extrathoracic, tracheo-bronchial, and alveolar regions respectively while the total dosage was overpredicted by 5.86% when using the square wave patterns. Table 5.11 shows the predicted dosage as a percent of the initial nebulizer charge using nebulizer and square breathing patterns. Separately these discrepancies may be tolerable but, when combined, result in an unacceptable overprediction of the amount of saline depositing in each lung region. Consequently, the use of square wave flow patterns should be avoided in nebulizer testing.

	Dosage as Percent of Initial Nebulizer Charge			
Breathing Pattern	ET (%)	TB (%)	AL (%)	TOT (%)
nebulizer	4.31	4.04	3.51	11.86
square	5.18	4.73	4.60	14.50
Overprediction (%)	20.2	17.0	31.1	22.3

Table 5.11: Combined *in vitro* and TechAero square wave overprediction

5.4.4 Summary

No substantial differences in the regional lung deposition were observed as the result of variations in the functional shape of the breathing pattern. The deposition results for the nebulizer, normal, and sine waves in each set were often nearly the same with the majority of the discrepancy coming from the square wave results. Removing the initial particle size variability generally shifted the deposition percentages slightly but did not affect the differences between one breathing pattern relative to another.

On average, square wave flow patterns resulted in slight overprediction of both the regional dosages and the total amount of saline inhaled. The combined effect of these discrepancies result in consistent and significant dosage overpredictions.

Chapter 6

Conclusions

6.1 Synopsis

The purpose of this research was to scrutinize one aspect of nebulizer drug delivery with the goal of evaluating its significance in maintaining sufficient realism during *in vitro* testing. Specifically, we wished to examine the implications of using simplified breathing patterns in vented jet nebulizer testing. This report presented the three phases of this study: 1) The gathering of real human breathing patterns, breathing normally and through a nebulizer and the subsequent assessment of the changes introduced in breathing patterns due to breathing through a nebulizer. 2) The standardized bench testing that was done to examine the effect of breathing pattern variations on nebulizer output efficiency and particle size distributions. 3) The Eulerian computer simulation, TechAero, that was used to predict the effect of breathing pattern variations on the regional deposition in a modelled lung.

6.1.1 Real Breathing Patterns

A head-out full body plethysmograph was used to record subjects breathing normally and while breathing through a nebulizer. The resultant data traces were processed to obtain representative average waveforms for each subject's normal and nebulizer breathing. These average waveforms were then compared to determine the differences caused by breathing though a nebulizer.

Nebulizer breathing was observed to be significantly different from normal breathing tending to increase the tidal volume and lengthen the period of the breath, confirming previously published results. Additionally, the specific functional shape of human breathing

was also observed to change. In particular, breathing through a nebulizer tends to lengthen the inhale duration to a greater extent than the lengthening of the exhale duration. The consequence of this is a shift in the breath duty cycle. Breathing through a nebulizer tends to even out the phase durations resulting in the duty cycle approaching 50%. Also, the point at which maximum flow is reached during each breath phase was also shifted between normal and nebulizer breathing. Breathing through a nebulizer causes the maximum flow peak to be reached sooner in the inhale and later in the exhale. To examine the consequence of these differences, the breathing patterns were grouped into sets of normal, nebulizer, sine, and square waves according to each subject with those sets containing the most significant differences in the waveforms considered for inclusion in the second part of the study.

6.1.2 Bench Testing

Statistically significant variation in nebulizer output efficiency was observed for two of the six breath sets used in the bench testing. Incidentally, the breathing sets that caused nebulizer output differences were also the most significantly different waveforms. This suggests that breathing pattern variation is only significant above a certain level of difference in the waveforms. The square wave breathing patterns consistently produced higher output efficiencies than the other waveforms within a test set. For non-square waveforms, output efficiency appears to be affected by the location of the point of maximum flow in the inhale in that the sooner the maximum flow is reached the more the efficiency is reduced. Additionally, shorter breath duty cycles cause the exhale valve to be open for a larger fraction of the nebulization time resulting in more wasted aerosol to the environment and lower output efficiency. Also, the output differences that were observed appear to scale with the breath minute ventilation. For breathing pattern differences significant enough to cause output dissimilarity, the magnitude of the resultant differences decrease with a decrease in minute ventilation. It was also observed that a fairly significant degree of device variability existed among the nebulizers used. If the device variation is significant enough, that alone will cause output efficiency variation that would supersede any variation due to breathing pattern differences.

The output particle size was seen to be primarily affected by the average inspiratory flow through the device. The output MMD from the device decreases as the average flow rate

of the breathing pattern inhale increases. Within a test set, however, where all waveforms had identical minute ventilation and mean inspiratory flow, no significant differences in the average MMD was observed. Differences were observed, however, in the measured MMD during the course of a single breath. Due to the size dependence on flow rate through the device, larger particles are produced at the start of the breath while the flow rate is low. The particle size quickly falls to the test average during most of the inhale with indications that it then grows again near the end as the flow rate drops. Square wave breathing patterns generate a more constant output particle size due to the sharp discontinuities in flow with no gradual ramping up or down.

6.1.3 Regional Deposition

With differences in nebulizer output observed as the result of breathing pattern variation, the study continued by examining the consequence of these differences on regional deposition in the lung. No substantial variation was observed in the regional deposition percentages as the result of breathing pattern functional shape differences. The largest discrepancies were due to the square waves in each set which consistently resulted in the highest deposition percentages in all regions for all cases. With the square waves removed the variation drops to below 5% in all regions. Performing the simulation tests again with particle size variations eliminated shifted the regional deposition percentages slightly but had negligible effect on the already small variations within each test set.

Both the bench testing and the computer simulations showed slight overprediction when using square wave rather than real nebulizer patterns. The combination of the discrepancies from each stage, however, results in consistent statistically significant overprediction.

6.2 Future Work

This report has established that breathing pattern variation does not cause significant differences in aerosol drug delivery testing in all cases. A logical next step would be to collect real breathing patterns from diseased subjects. These diseased breathing patterns could be similarly tested using the *in vitro* bench test and further tested using a diseased lung model within TechAero.

Furthermore, this research could be extended by examining the difference causing aspects of the breathing patterns more specifically. Rather than obtaining breathing patterns from real human subjects, they could be manufactured according to specific shape elements under test. In this way, the duty cycle and flow peak location effects could be quantified precisely.

6.3 Summary

In conclusion, the goal of this research was to aid researchers in making informed decisions when selecting breathing patterns to use in nebulizer testing. Due to great interpersonal variability among human breathing patterns, some sort of simplification will always need to be implemented. Yet it has been shown that several simplifications commonly used may produce inaccurate results. A square wave pattern overvalues output efficiency and regional deposition percentages and produces results farthest from those obtained with real nebulizer breathing patterns. Consequently, the use of constant flow square waves should be avoided. It was also shown that normal and sine waveforms produced quite similar results yet still overvalue output efficiency when compared with real nebulizer breathing. It was also shown that these breathing pattern differences do not cause output differences in all cases.

Ideally, test breathing patterns would approximate nebulizer breathing waveshape as closely as possible. If a simple standard waveform is to be used, a sine wave shifted to an appropriate human breathing duty cycle is preferred. Even more rigorous attempts to approximate real breathing using sine waves could be done by shifting the inhale flow peak to a more appropriate value.

Bibliography

[1] K. Stapleton and W. Finlay. Deposition of medical aerosols in the respiratory tract. Report MA-1, Department of Mechanical Engineering, University of Alberta, Edmonton, Alberta, 1997.

[2] W. H. Finlay. *The Mechanics of Inhaled Pharmaceutical Aerosols: An Introduction.* Academic Press, London, 2001.

[3] G. C. Smaldone. Drug delivery by nebulization: "Reality testing". *J. Aerosol Med.*, 7(3):213–216, 1994.

[4] K. Nikander, J. Denyer, M. Everard, and G. C. Smaldone. Validation of a new breathing simulator generating and measuring inhaled aerosol with adult breathing patterns. *J. Aerosol Med.*, 13(2):139–146, 2000.

[5] J. H. Dennis, S. C. Stenton, J. R. Beach, A. J. Avery, E. H. Walters, and D. J. Hendrick. Jet and ultrasonic nebulizer output: Use of a new method for direct measurement of aerosol output. *Thorax*, 45:728–732, 1990.

[6] R. Tandon, M. McPeck, and G. Smaldone. Measuring nebulizer output: Aerosol production vs gravimetric analysis. *Chest*, 111(5):1361–1365, 1997.

[7] D. Hess, D. Fisher, P. Williams, S. Pooler, and R. Kacmarek. Medication nebulizer performance: Effects of diluent volume, nebulizer flow, and nebulizer brand. *Chest*, 110(2):498–505, 1996.

[8] M. McPeck, R. Tandon, K. Hughes, and G. Smaldone. Aerosol delivery during continuous nebulization. *Chest*, 111(5):1200–1205, 1997.

[9] K. Nikander, J. Denyer, and G. C. Smaldone. Effects of equipment dead space and pediatric breathing patterns on inhaled mass of nebulized budesonide. *J. Aerosol Med.*, 12(2):67–73, 1999.

[10] J. H. Dennis. Drug nebulizer design and performance: Breath enhanced jet vs. constant output jet vs. ultrasonic. *J. Aerosol Med.*, 8(3):277–280, 1995.

[11] M J. O'Doherty, S. H. L. Thomas, C. J. Page, D. F. Treacher, and T. O. Nunan. Delivery of a nebulized aerosol to a lung model during mechanical ventilation. *Am. Rev. Respir. Dis.*, 146:383–388, 1992.

[12] T. G. O'Riordan, M. J. Greco, R. J. Perry, and G. C. Smaldone. Nebulizer function during mechanical ventilation. *Am. Rev. Respir. Dis.*, 145:1117–1122, 1992.

[13] P. J. Anderson. Respiratory drug delivery. *Chest*, 111(5):1155–1156, 1997.

[14] G. Benchetrit, S. A. Shea, T. P. Dinh, S. Bodocco, P. Baconnier, and A. Guz. Individuality of breathing pattern in adults assesed over time. *Respir. Physiol.*, 75:199–210, 1989.

[15] R. M. Prokop, W. H. Finlay, K. W. Stapleton, and P. Zuberbuhler. The effect of ambient relative humidity on regional dosages delivered by a jet nebulizer. *J. Aerosol Med.*, 8(4):363–372, 1995.

[16] M. Clay, D. Pavia, S. P. Newman, and S. W. Clarke. Factors influencing the size distribution of aerosols from jet nebulizers. *Thorax*, 38:755–759, 1983.

[17] C. Mundo, M. Sommerfeld, and C. Tropea. Droplet-wall collisions: experimental studies of the deformation and breakup process. *Int. J. Multiphase Flow*, 21:151–173, 1995.

[18] A. L. Yarin and D. A. Weiss. Impact of drops on solid surfaces: self-similar capillary waves, and splashing as a new type of kinematic discontinuity. *J. Fluid Mech.*, 283:141–173, 1995.

[19] W. H. Finlay, M. Hoskinson, and K. W. Stapleton. Can models be trusted to subdivide lung deposition into alveolar and tracheobronchial fractions? In *Respiratory Drug Delivery VI*, pages 235–242, Buffalo Grove, IL, USA, 1998. Interpharm Press.

[20] M. J. Tobin, T. S. Chadha, G. Jenouri, S. Birch, H. B. Gazeroglu, and M. A. Sackner. Breathing patterns 1: Normal subjects. *Chest*, 84(2):202–205, 1983.

[21] M. J. Tobin, T. S. Chadha, G. Jenouri, S. Birch, H. B. Gazeroglu, and M. A. Sackner. Breathing patterns 2: Diseased subjects. *Chest*, 84(3):286–294, 1983.

[22] J. D. Sackner, A. J. Nixon, B. Davis, and N. Atkins. Effects of breathing through external dead space on ventilation at rest and during exercise. *Am. Rev. Respir. Dis.*, 122:933–940, 1980.

[23] D. Paek and D. McCool. Breathing patterns during varied activities. ii. *J. Appl. Physiol.*, 73(3):887–893, 1992.

[24] P. Fleming, M. R. Levine, and A. Goncalves. Changes in respiratory pattern resulting from the use of a facemask to record respiration in newborn infants. *Pediatr. Res.*, 16:1031–1034, 1982.

[25] J. Askanzi, P. A. Silverberg, R. J. Foster, A. I. Hyman, J. Milic-Emili, and J. M. Kinney. Effects of respiratory apparatus on breathing pattern. *J. Appl. Physiol.*, 48(4):577–580, 1980.

[26] R. Gilbert, J. H. Auchincloss Jr., J. Brodsky, and W. Boden. Changes in tidal volume, frequency, and ventilation induced by their measurement. *J. Appl. Physiol.*, 33(2):252–254, 1972.

[27] W. Perez and M. Tobin. Separation of factors responsible for change in breathing pattern induced by instrumentation. *J. Appl. Physiol.*, 59(5):1515–1520, 1985.

[28] W. H. Finlay, K. W. Stapleton, and P. Zuberbuhler. Variations in predicted regional lung deposition of salbutamol sulphate between 19 nebulizer models. *J. Aerosol Med.*, 11:65–80, 1998.

[29] C. F. Lange and W. H. Finlay. A fully eulerian approach to the simulation of volatile/hygroscopic aerosols. In *A CFD Odyssey*. CFD Society of Canada, 2001.

[30] D. A. Edwards. The macrotransport of aerosol particles in the lung: Aerosol deposition phenomena. *J. Aerosol Sci.*, 26(2):293–317, 1995.

[31] W. H. Finlay, C. F. Lange, C. F. King, and D. Speert. Lung delivery of aerosolized dextran. *Am. J. Resp. Crit. Care Med.*, 161:91–97, 2000.

[32] C. G. Phillips, S. R. Kaye, and R. C. Schroter. A diameter-based reconstruction of the branching pattern of the human bronchial tree. Part I: Description and application. *Respir. Physiol.*, 98:193–217, 1994.

[33] C. G. Phillips, S. R. Kaye, and R. C. Schroter. A diameter-based reconstruction of the branching pattern of the human bronchial tree. Part II: Mathematical formulation. *Respir. Physiol.*, 98:219–226, 1994.

[34] B. Haefeli-Bleuer and E. R. Weibel. Morphometry of the human pulmonary acinus. *Anat. Rec.*, 220:401–414, 1988.

[35] H. L. Stone. Iterative solution of implicit approximations of multi-dimensional partial differential equations. *SIAM J. Num. Anal.*, 5:530–558, 1968.

[36] H. Smith, editor. *Human respiratory tract model for radiological protection*, volume ICRP publication 66 of *Annals of the ICRP*. Pergamon, Oxford, 1994.

[37] T. L. Chan and M. Lippmann. Experimental measurements and empirical modelling of the regional deposition of inhaled particles in humans. *Am. Ind. Hyg. Assoc. J.*, 41:399–409, 1980.

[38] J. Pich. Theory of gravitational deposition of particles from laminar flows in channels. *j. Aerosol Sci.*, 3:351–361, 1972.

[39] J. Heyder and J. Gebhart. Gravitational deposition of particles from laminar aerosol flow through inclined circular tubes. *J. Aerosol Sci.*, 8:289–295, 1977.

[40] D. B. Ingham. Diffusion of aerosols from a stream flowing through a cylindrical tube. *J. Aerosol Sci.*, 6:125–132, 1975.

[41] P. G. Gormley and K. Kennedy. Diffusion from a stream flowing through a cylindrical tube. *Proc. Roy. Irish Soc.*, 52A:163, 1949.

[42] P-Y. Carry, P. Baconnier, A. Eberhard, P. Cotte, and G. Benchetrit. Evaluation of respiratory inductive plethysmography: Accuracy for analysis of respiratory waveforms. *Chest*, 111(4):910–915, 1997.

[43] O. G. Raabe. The dilution of monodisperse suspensions for aerosolization. *Am. Ind. Hyg. Assoc. J.*, 6(16):439–443, 1968.

[44] P. C. Emmett, R. J. Aitken, and W. J. Hannan. Measurements of the total and regional deposition of inhaled particles in the human respiratory tract. *J. Aerosol Sci.*, 13(6):549–560, 1972.

[45] N. Foord, A. Black, and M. Walsh. Regional deposition of 2.5 – 7.5μm diameter inhaled particles in healthy male non-smokers. *J. Aerosol Sci.*, 9:343–357, 1978.

[46] M. Lippmann and R. E. Albert. The effect of particle size on the regional deposition in the human respiratory tract. *Am. Ind. Hyg. Assoc. J.*, 30:357–375, 1969.

[47] R. V. Lourenco, M. F. Klimek, and C. J. Borowski. Deposition and clearance of 2μm particles in the tracheobronchial tree of normal subjects – smokers and non-smokers. *J. of Clinical Investigation*, 50:1411–1420, 1971.

[48] G. Taylor. Dispersion of soluble matter in solvent flowing slowly through a tube. *Proc. Roy. Soc. London, Ser. A*, 219:186–203, 1953.

[49] K. W. Stapleton, W. H. Finlay, and P. Zuberbuhler. An in-vitro method for determining regional dosages delivered by jet nebulizers. 7(4):325–344, 1994.

Appendix A

Sample TechAero I/O

```
Phillips&al.+Haefeli_Bleuer&Weibel/3.05 litres
~~~~~~~~~~~~~~~~~~~~~~~~~~~~~~~~~~~~~~~~~~~~~~~~~~~~~~~~~~~~~~~~~~~~~~~~~~~~
3  18  26                    ! TracheaGen, AlveolGenStart, LungGenTotal
 1  10.100   1.750    24.290  ! Oral cavity+oropharyngeal region  (gen,length[cm],diam.[cm],accum.vol.[cc])
 2   8.000   2.000    49.420  ! pharynx+larynx
 3  12.456   1.810    81.470  ! trachea (beginning of TB_region)
 4   3.614   1.414    92.821
 5   2.862   1.115   103.992
 6   2.281    .885   115.206
 7   1.780    .706   126.338
 8   1.126    .565   135.368
 9    .897    .454   144.657
10    .828    .364   155.656
11    .745    .286   167.878
12    .653    .218   180.342
13    .555    .162   192.131
14    .454    .121   202.801
15    .357    .092   212.539
16    .277    .073   222.064
17    .219    .061   232.550
18    .134    .049   254.387  ! beginning of alveolar region
19    .109    .048   289.318
20    .091    .039   333.521
21    .081    .037   407.313
22    .068    .035   523.466
23    .068    .033   739.292
24    .068    .030  1117.127
25    .065    .028  1792.162
26    .073    .024  3049.420
__ End of input part __
Comments:
 Lung Model used:   trachea (gen. 3) to gen. 17 is Phillips et al.+
 gen. 18_26 is  Haefeli_Bleuer&Weibel, corrected for 3050 cc lung volume (51% of TLC).
 NOTE: the above gen. numbers, using traditional numbering (with gen. 0 being
  the trachea), give 0_14 conducting airways and 15_23 the alveolated region.
```

Figure A.1: The hybrid lung model used in TechAero

```
#  INPUT DATA FILE FOR TECHAERO (don't delete comment lines!)
#  (next line is the Problem Title [max. 80 chars.])
manual calculation test (pure inhalation, U=0.001 m/s)
0.93              # program version
# ____ Discretization Parameters ____
t f f f          # logical flags for variables to compute (Count,T,Cinf,Tinf)
f                 # logical flag for hygroscopicity
100   30          # number of grid points in x and R directions
1.d_2             # time step [s]
15                # max. no. of iterations per time step
1.0d_1            # time between plot outputs [s]
0.0d0             # time discretization factor (expl=0;Cr_Nic=0.5;impl=1)
0.0d0             # convective discretization blending factor (UDS=0;CDS=1)
1.d0 .8d0 1.d0 1.d0     # under_relaxation factors for Count,T,Cinf,Tinf
1.d_4             # convergence tolerance
# ____ Ambient and Physiological Data ____
/home2/clange/techaero/philhaef.dat     # path and file name for the lung model [max. 80 chars.]
 3.d0  2.d0      # mouthpiece dimensions (length, equiv. diam.) [cm]
20.  50.          # ambient temp [oC], ambient RH [%]
15.0d0            # breaths/min
1                 # number of breath cycles to compute
30.0d0            # max. inhalation flow rate [l/min]
50.d0  0.d0       # % time inhaling, % time holding
1.                # mouth breathing fraction
0. 2. 18. 1.70  # scaling of lung geometry (flag [scale=1],sex[f=1;m=2],age[yrs],height[m])
0   f             # pediatric lung: age [mo. or 0=adult], flag for stand. ped. brthng. (overrides input data)
f   f             # log. flags for: reading breath input file, scaling input breath function
# ____ Aerosol Data ____
NaCl              # name of solute compound 1 [max. 12 chars.]
x                 # name of solute compound 2 [max. 12 chars.]
x                 # name of solute compound 3 [max. 12 chars.]
x                 # name of solute compound 4 [max. 12 chars.]
10.0  0. 0. 0.  # initial conc. for each compound(4) [mg/ml=kg/m3] (use density if solid particle)
2170.0 0. 0. 0. # density of each compound(4) [kg/m3]
920.0  0. 0. 0. # specific heat of each compound(4) [J/(kg K)]
26.3  0. 0. 0.  # solubility of each compound(4) [%w/w]
58.45 0. 0. 0.  # mol. weight of each compound(4) [g/mol=kg/kmol] (set to 0 for non_ideal chem.)
1.8  0. 0. 0.   # van't Hoff factor for each compound(4) (set to 0 for non_ideal chem.)
2.d0  16.d0       # lower and upper cuttoff diameters [microns]
t  f  f          # logical flags for: initially lognormal, initially monodisperse, pure solvent(no solute)
f  f              # logical flags for time dependence of: particle production rate, size distrib. parameters
6.d0 1.4d0        # initial MMD or monodisperse diameter [microns], initial GSD
2.5d3             # max. particle production rate at inhalation [1/s]
20.d0             # droplets' temperature at inhalation [oC]
```

Figure A.2: Example TechAero *input.dat* file

```
99
0 0
0.02205386  1.7719632
0.04410771  3.8082882
0.06616158  6.0808014
0.08821544  8.5655136
0.11026931  11.2396302
0.13232313  13.9935198
0.15437706  16.7749278
0.17643088  19.6279452
0.1984847   22.4914848
0.22053862  25.3007784
0.24259245  28.0044276
0.26464627  30.5461596
0.28670019  32.8752984
0.30875401  34.9478328
0.33080784  36.7273758
0.35286176  38.1876528
0.37491558  39.3132666
0.3969695   40.0998312
0.41902333  40.5543174
0.44107715  40.6947006
0.46313107  40.5481806
0.48518489  40.1496432
0.50723872  39.53994
0.52929254  38.7631254
0.55134646  37.8639342
0.57340038  36.8854836
0.59545421  35.8665558
0.61750803  34.8395304
0.63956185  33.8290116
0.66161577  32.8502916
0.6836696   31.9086078
0.70572352  30.9996414
0.72777734  30.1100352
0.74983116  29.2181934
0.77188499  28.2964146
0.79393891  27.3129786
0.81599283  26.2342068
0.83804665  25.0271106
0.86010048  23.6618088
0.8821543   22.1134344
0.90420822  20.36427
0.92626204  18.4052376
0.94831597  16.236393
```

Figure A.3: Example *breath.dat* input file

```
#      x          cell size   ; no. of points=   200
  1  0.00000E+00  1.00000E_90
  2  1.80769E_03  3.61538E_03
  3  5.42308E_03  3.61538E_03
  4  9.03846E_03  3.61538E_03
  5  1.26538E_02  3.61538E_03
  6  1.62692E_02  3.61538E_03
  7  1.98846E_02  3.61538E_03
  8  2.35000E_02  3.61538E_03
  9  2.71154E_02  3.61538E_03
 10  3.07308E_02  3.61538E_03
 11  3.43462E_02  3.61538E_03
 12  3.79615E_02  3.61538E_03
 13  4.15769E_02  3.61538E_03
 14  4.51923E_02  3.61538E_03
 15  4.88704E_02  3.74074E_03
 16  5.26111E_02  3.74074E_03
 17  5.63519E_02  3.74074E_03
 18  6.00926E_02  3.74074E_03
 19  6.38333E_02  3.74074E_03
 20  6.75741E_02  3.74074E_03
 21  7.13148E_02  3.74074E_03
 22  7.50556E_02  3.74074E_03
 23  7.87963E_02  3.74074E_03
 24  8.25370E_02  3.74074E_03
 25  8.62778E_02  3.74074E_03
 26  9.00185E_02  3.74074E_03
 27  9.37593E_02  3.74074E_03
 28  9.75000E_02  3.74074E_03
 29  1.01241E_01  3.74074E_03
 30  1.04981E_01  3.74074E_03
 31  1.08722E_01  3.74074E_03
 32  1.12463E_01  3.74074E_03
 33  1.16204E_01  3.74074E_03
 34  1.19944E_01  3.74074E_03
 35  1.23685E_01  3.74074E_03
 36  1.27426E_01  3.74074E_03
 37  1.31167E_01  3.74074E_03
 38  1.34907E_01  3.74074E_03
 39  1.38648E_01  3.74074E_03
 40  1.42389E_01  3.74074E_03
 41  1.46130E_01  3.74074E_03
 42  1.49818E_01  3.63636E_03
 43  1.53455E_01  3.63636E_03
 44  1.57091E_01  3.63636E_03
```

Figure A.4: Example *grid.out* output file

```
#gen.    x[cm]      specif.dos.[mg/cm]   specif.solv.[mg/cm]  _ Breathing pattern testing
for: Brads_nbnm
  1   1.80769E_01   0.00000E+00          0.00000E+00
  1   5.42308E_01   0.00000E+00          0.00000E+00
  1   9.03846E_01   0.00000E+00          0.00000E+00
  1   1.26538E+00   0.00000E+00          0.00000E+00
  1   1.62692E+00   0.00000E+00          0.00000E+00
  1   1.98846E+00   0.00000E+00          0.00000E+00
  1   2.35000E+00   0.00000E+00          0.00000E+00
  1   2.71154E+00   0.00000E+00          0.00000E+00
  1   3.07308E+00   0.00000E+00          0.00000E+00
  1   3.43462E+00   0.00000E+00          0.00000E+00
  1   3.79615E+00   0.00000E+00          0.00000E+00
  1   4.15769E+00   0.00000E+00          0.00000E+00
  1   4.51923E+00   0.00000E+00          0.00000E+00
  2   4.88704E+00   0.00000E+00          1.85385E_05
  2   5.26111E+00   0.00000E+00          1.85540E_05
  2   5.63519E+00   0.00000E+00          1.85696E_05
  2   6.00926E+00   0.00000E+00          1.85855E_05
  2   6.38333E+00   0.00000E+00          1.86017E_05
  2   6.75741E+00   0.00000E+00          1.86183E_05
  2   7.13148E+00   0.00000E+00          1.86354E_05
  2   7.50556E+00   0.00000E+00          1.86528E_05
  2   7.87963E+00   0.00000E+00          1.86707E_05
  2   8.25370E+00   0.00000E+00          1.86890E_05
  2   8.62778E+00   0.00000E+00          1.87078E_05
  2   9.00185E+00   0.00000E+00          1.87270E_05
  2   9.37593E+00   0.00000E+00          1.87467E_05
  2   9.75000E+00   0.00000E+00          1.87668E_05
  2   1.01241E+01   0.00000E+00          1.87874E_05
  2   1.04981E+01   0.00000E+00          1.88085E_05
  2   1.08722E+01   0.00000E+00          1.88301E_05
  2   1.12463E+01   0.00000E+00          1.88522E_05
  2   1.16204E+01   0.00000E+00          1.88748E_05
  2   1.19944E+01   0.00000E+00          1.88980E_05
  2   1.23685E+01   0.00000E+00          1.89217E_05
  2   1.27426E+01   0.00000E+00          1.89460E_05
  2   1.31167E+01   0.00000E+00          1.89710E_05
  2   1.34907E+01   0.00000E+00          1.89967E_05
  2   1.38648E+01   0.00000E+00          1.90231E_05
  2   1.42389E+01   0.00000E+00          1.90506E_05
  2   1.46130E+01   0.00000E+00          1.90796E_05
  3   1.49818E+01   0.00000E+00          2.48804E_05
  3   1.53455E+01   0.00000E+00          2.48310E_05
  3   1.57091E+01   0.00000E+00          2.47811E_05
```

Figure A.5: Example *locdep.out* output file

#gen. dosage[mg] dosage[%] solv.dose[mg] solv.dose[%] _ Breathing pattern testing for: Brads_nbnm

1	0.00000E+00	0.000	0.00000E+00	0.000
2	0.00000E+00	0.000	1.89694E_04	14.044
3	0.00000E+00	0.000	1.94446E_04	14.396
4	0.00000E+00	0.000	1.45155E_05	1.075
5	0.00000E+00	0.000	1.70848E_05	1.265
6	0.00000E+00	0.000	1.74134E_05	1.289
7	0.00000E+00	0.000	1.76309E_05	1.305
8	0.00000E+00	0.000	1.77258E_05	1.312
9	0.00000E+00	0.000	1.69025E_05	1.251
10	0.00000E+00	0.000	1.69865E_05	1.258
11	0.00000E+00	0.000	1.82013E_05	1.348
12	0.00000E+00	0.000	2.01901E_05	1.495
13	0.00000E+00	0.000	2.29318E_05	1.698
14	0.00000E+00	0.000	2.61845E_05	1.939
15	0.00000E+00	0.000	2.91378E_05	2.157
16	0.00000E+00	0.000	3.11960E_05	2.310
17	0.00000E+00	0.000	3.19509E_05	2.366
18	0.00000E+00	0.000	3.23441E_05	2.395
19	0.00000E+00	0.000	6.82735E_05	5.055
20	0.00000E+00	0.000	6.20520E_05	4.594
21	0.00000E+00	0.000	5.98013E_05	4.427
22	0.00000E+00	0.000	4.74239E_05	3.511
23	0.00000E+00	0.000	1.25242E_05	0.927
24	0.00000E+00	0.000	4.82263E_07	0.036
25	0.00000E+00	0.000	7.82667E_10	0.000
26	0.00000E+00	0.000	5.39784E_14	0.000
27	0.00000E+00	0.000	2.77859E_19	0.000

Figure A.6: Example *gendep.out* output file

```
                    TechAero
  Truly Eulerian Code for simulation of Hygroscopic AEROsols.
                   Version 0.93
Copyright 1999,2000 Aerosol Research Laboratory of Alberta, U. of A.

Title of the run:
Breathing pattern testing for: Brads_snnm

Computation Parameters:
 Computed: count_distr.
 Number of grid points:   200 in X,    50 in R and     3 in MS.
 Time step [s]:  1.000E_04
 Time discret. factor:  1.00
 Convection discret. factor:  0.00

Ambient and Physiological Data:
 Lung geometry model: Phillips&al.+Haefeli_Bleuer&Weibel/3.05 litres
 Mouthpiece dimensions (L,D)[cm]:  4.700  1.400
 Ambient temperature [oC]:  23.000
 Ambient humidity [%]:  50.000
 Lung corresponds to an adult at 50% TLC.
 Breath function read in from file.
 Input breath parameters overridden by input breath function.
 Inhalation volume [l]:  0.454
 Breaths per minute:  19.822
 Number of breath cycles:  1
 Inhal., breath hold, exhal. [%]:  35.70,  0.00,  64.30
 Mouth breathing fraction [%]:  1.00

Aerosol Data:
 Particles of pure: water
 Total amount inhaled [ml]:  1.351E_03
 Lognormal distributed aerosol.
 Initial MMD [microns]:  5.060E+00
 Initial GSD:  1.600E+00

Regional dosages [mg | %]:
(percentages of total inhaled =  1.351E_03 mg)
 Extra_thoracic:     3.768E_04 |  27.90
 Tracheo_bronchial:  3.272E_04 |  24.22
 Alveolar:           2.720E_04 |  20.14
 Total dosage:       9.760E_04 |  72.26
```

Figure A.7: Example *regdep.out* output file

Appendix B

Raw Data

Normal Breathing	Tidal Volume (L)	Total Time (s)	Frequency (breaths/min)	Minute Ventilation (L/min)
Alexz	0.877	3.87	15.504	13.597
Brads	0.471	3.05	19.672	9.266
Colinn	0.637	2.72	22.059	14.051
Davide	0.673	3.11	19.293	12.984
Keanz	0.671	3.29	18.237	12.237
Keng	0.626	3.53	16.997	10.640
Kevinm	0.699	3.65	16.438	11.490
Marcr	0.652	2.71	22.140	14.435
Mikem	0.500	2.83	21.201	10.601
Robp	0.572	3.57	16.807	9.613
Shawnt	0.460	3.11	19.293	8.875
Troys	0.512	3.49	17.192	8.802
Average	0.613	3.24	18.736	11.383
StdDev	0.119	0.38	2.242	2.053
Nebulizer Breathing	Tidal Volume (L)	Total Time (s)	Frequency (breaths/min)	Minute Ventilation (L/min)
Alexz	0.908	4.59	13.072	11.869
Brads	0.495	3.22	18.634	9.224
Colinn	0.681	3.62	16.575	11.287
Davide	1.391	5.29	11.342	15.777
Keanz	0.952	4.42	13.575	12.923
Keng	0.831	6.18	9.709	8.068
Kevinm	0.774	4.51	13.304	10.297
Marcr	0.846	4.31	13.921	11.777
Mikem	0.695	5.44	11.029	7.665
Robp	0.493	3.88	15.464	7.624
Shawnt	0.365	2.85	21.053	7.684
Troys	1.055	4.29	13.986	14.755
Average	0.791	4.38	14.305	10.746
StdDev	0.279	0.94	3.229	2.813

Table B.1: Average breath parameters for each subject

Difference Neb-Norm	Tidal Volume (L)	Total Time (s)	Frequency (breaths/min)	Minute Ventilation (L/min)
Alexz	0.031	0.720	-2.432	-1.728
Brads	0.024	0.170	-1.039	-0.042
Colinn	0.044	0.900	-5.484	-2.764
Davide	0.718	2.180	-7.950	2.793
Keanz	0.281	1.130	-4.662	0.686
Keng	0.205	2.650	-7.288	-2.572
Kevinm	0.075	0.860	-3.135	-1.193
Marcr	0.194	1.600	-8.219	-2.658
Mikem	0.195	2.610	-10.172	-2.935
Robp	-0.079	0.310	-1.343	-1.990
Shawnt	-0.095	-0.260	1.760	-1.190
Troys	0.543	0.800	-3.206	5.953
Average	0.178	1.139	-4.431	-0.637
StdDev	0.243	0.942	3.511	2.673

Table B.2: Difference in means for each subject – To be used for matched pair analysis

Normal Breathing	Tidal Volume (L)	Total Time (s)	Frequency (breaths/min)	Minute Ventilation (L/min)	Inhale Time (s)	Exhale Time (s)	Duty Cycle	Inhale Flow Peak	Exhale Flow Peak	Mean Insp Flow (L/min)
Alexz	0.772	3.391	17.694	13.657	1.411	1.980	0.416	0.612	0.204	32.815
Brads	0.454	3.027	19.824	9.004	1.081	1.946	0.357	0.408	0.184	25.212
Colinn	0.612	2.701	22.215	13.598	1.270	1.431	0.470	0.347	0.204	28.918
Davide	0.631	3.041	19.728	12.455	1.151	1.891	0.378	0.367	0.184	32.917
Keanz	0.514	2.930	20.478	10.526	1.596	1.334	0.545	0.612	0.306	19.326
Keng	0.646	2.872	20.894	13.495	1.208	1.664	0.421	0.714	0.184	32.086
Kevinm	0.550	3.334	17.995	9.903	1.396	1.938	0.419	0.449	0.204	23.645
Marcr	0.681	2.357	25.453	17.323	0.993	1.364	0.421	0.449	0.225	41.107
Mikem	0.468	2.743	21.875	10.244	1.069	1.674	0.390	0.449	0.204	26.297
Robp	0.511	3.349	17.918	9.158	1.372	1.977	0.410	0.429	0.204	22.356
Shawnt	0.435	2.891	20.757	9.027	1.245	1.646	0.431	0.531	0.265	20.966
Troys	0.529	3.403	17.632	9.320	1.519	1.884	0.446	0.429	0.306	20.881
Average	0.567	3.003	20.205	11.476	1.276	1.727	0.425	0.483	0.223	27.211
StdDev	0.102	0.324	2.309	2.620	0.187	0.244	0.048	0.111	0.045	6.510
Nebulizer Breathing	Tidal Volume (L)	Total Time (s)	Frequency (breaths/min)	Minute Volume (L/min)	Inhale Time (s)	Exhale Time (s)	Duty Cycle	Inhale Flow Peak	Exhale Flow Peak	Mean Insp Flow (L/min)
Alexz	0.810	4.373	13.720	11.107	2.074	2.299	0.474	0.531	0.265	23.421
Brads	0.422	2.992	20.053	8.463	1.474	1.519	0.493	0.306	0.367	17.184
Colinn	0.630	3.454	17.370	10.936	1.693	1.761	0.490	0.286	0.306	22.314
Davide	1.379	5.264	11.399	15.714	2.610	2.654	0.496	0.265	0.265	31.691
Keanz	0.785	3.812	15.741	12.363	2.039	1.772	0.535	0.204	0.327	23.107
Keng	0.717	5.743	10.448	7.488	2.152	3.591	0.375	0.327	0.388	19.986
Kevinm	0.794	4.471	13.421	10.659	1.837	2.634	0.411	0.408	0.286	25.947
Marcr	0.779	3.692	16.250	12.657	1.683	2.009	0.456	0.408	0.347	27.770
Mikem	0.776	5.248	11.432	8.868	2.325	2.924	0.443	0.388	0.531	20.022
Robp	0.558	3.761	15.953	8.897	2.021	1.740	0.537	0.327	0.306	16.556
Shawnt	0.378	2.975	20.167	7.629	1.367	1.609	0.459	0.347	0.286	16.609
Troys	1.097	4.417	13.584	14.900	2.506	1.911	0.567	0.367	0.286	26.258
Average	0.760	4.184	14.961	10.807	1.982	2.202	0.478	0.347	0.330	22.572
StdDev	0.273	0.898	3.211	2.711	0.389	0.631	0.055	0.083	0.074	4.769

Table B.3: Average breath parameters for a segment of data from each subject

Difference *Neb-Norm*	Tidal Volume (L)	Total Time (s)	Frequency (breaths/min)	Minute Ventilation (L/min)	Inhale Time (s)	Exhale Time (s)	Duty Cycle	Inhale Flow Peak	Exhale Flow Peak	Mean Insp. Flow (L/min)
Alexz	0.038	0.982	-3.975	-2.549	0.663	0.320	0.058	-0.082	0.061	-9.393
Brads	-0.032	-0.035	0.230	-0.541	0.393	-0.427	0.135	-0.102	0.184	-8.029
Colinn	0.018	0.753	-4.845	-2.662	0.423	0.331	0.020	-0.061	0.102	-6.604
Davide	0.747	2.223	-8.330	3.260	1.459	0.763	0.117	-0.102	0.082	-1.227
Keanz	0.271	0.882	-4.737	1.837	0.444	0.438	-0.010	-0.408	0.020	3.781
Keng	0.071	2.871	-10.446	-6.007	0.944	1.927	-0.046	-0.388	0.204	-12.100
Kevinm	0.244	1.136	-4.573	0.757	0.440	0.696	-0.008	-0.041	0.082	2.302
Marcr	0.098	1.335	-9.202	-4.666	0.690	0.646	0.034	-0.041	0.122	-13.337
Mikem	0.307	2.505	-10.442	-1.376	1.256	1.249	0.053	-0.061	0.327	-6.274
Robp	0.047	0.413	-1.966	-0.261	0.649	-0.237	0.128	-0.102	0.102	-5.800
Shawnt	-0.057	0.085	-0.590	-1.398	0.122	-0.037	0.029	-0.184	0.020	-4.357
Troys	0.568	1.014	-4.048	5.580	0.988	0.027	0.121	-0.061	-0.020	5.377
Average	0.193	1.180	-5.244	-0.669	0.706	0.475	0.053	-0.136	0.107	-4.638
StdDev	0.249	0.921	3.638	3.247	0.390	0.654	0.061	0.128	0.095	6.064

Table B.4: Difference in means for each subject – To be used for matched pair analysis

Appendix C

Program Algorithms

The following pages contain algorithm flowcharts for the different programs written for this study.

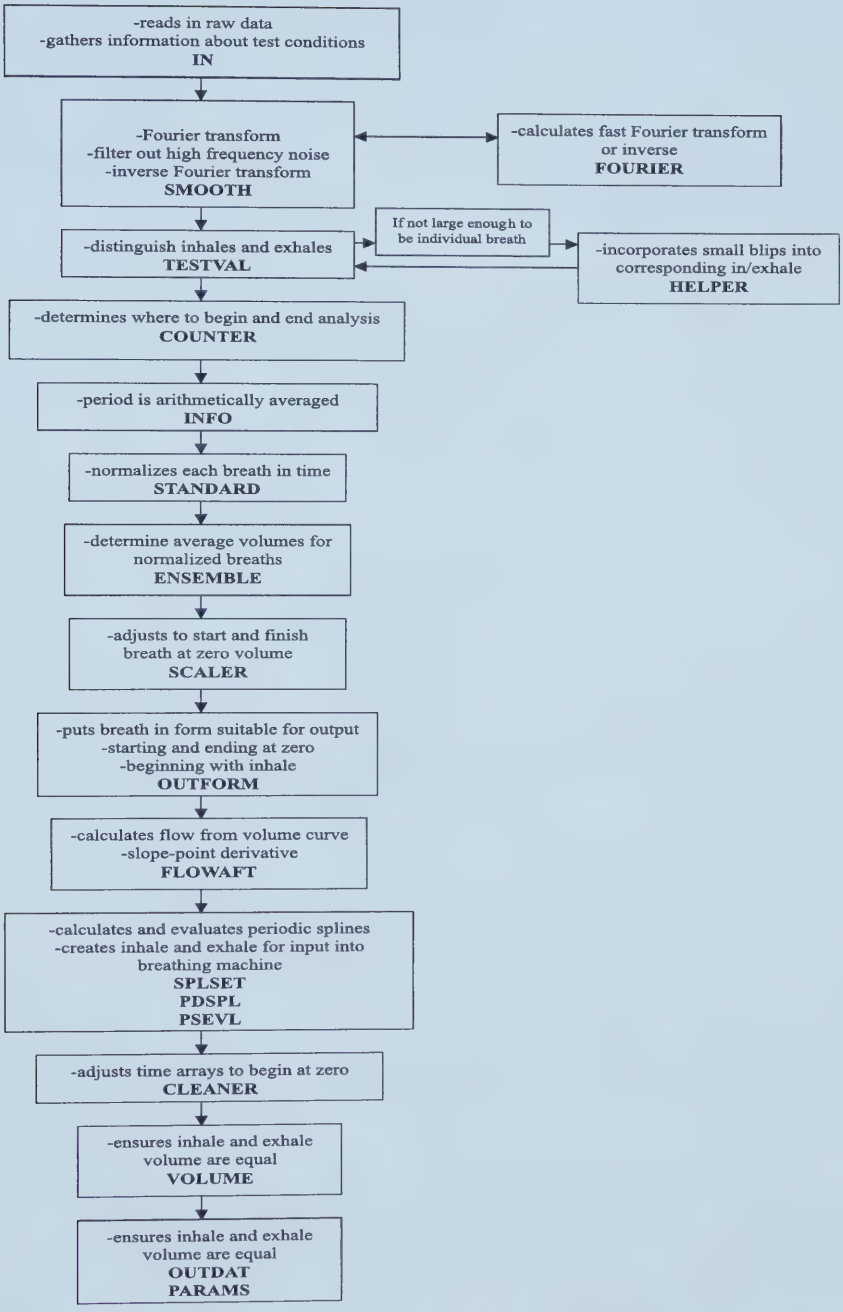

Figure C.1: Summary of the algorithm used in calculating the representative average breath

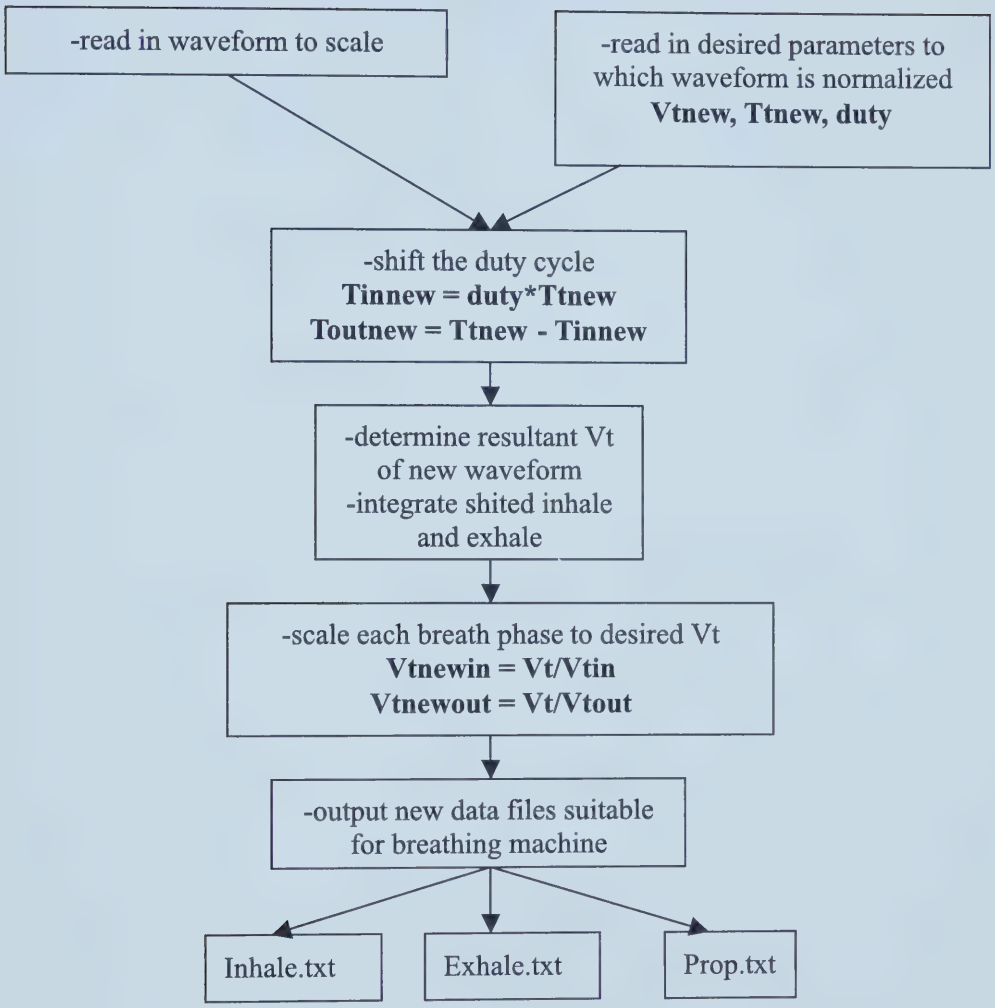

Figure C.2: The Matlab script *scalerflow.m* used to normalize the breathing patterns to specific V_T, T_T, and duty cycle

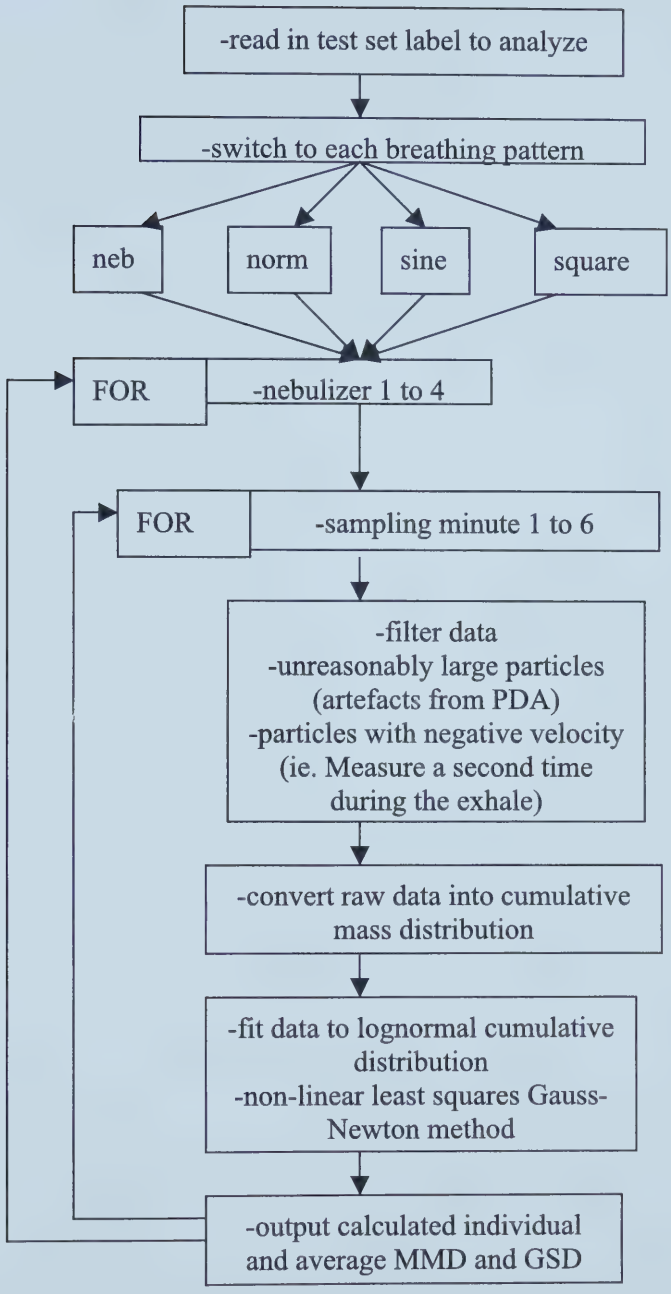

Figure C.3: The Matlab script *sizer.m* used calculate the MMD and GSD for PDA size size measurements